8-11-2020

Math Modeling of Interlimb Coordination in Cat Locomotion

Elizaveta Latash

MATH MODELING OF INTERLIMB COORDINATION IN CAT LOCOMOTION

by

ELIZAVETA LATASH

Under the Direction of Yaroslav Molkov, PhD

ABSTRACT

Locomotion is an evolutionary adaptation that allows animals to move in 3-D space. The way that mammalian locomotion is controlled has been studied for generations. It remains unclear how the neuronal network that controls locomotion is structured and how the mammalian locomotor network keeps balance in the face of a changing environment. In this body of research, we build mathematical models of locomotion and fit our models to experimental data of walking cats to gain understanding of network connectivity and of balance control. Specifically, we test the biological plausibility of a particular connectivity of the mammalian locomotor network by matching network activity to phases of walking in different experimental conditions. We gain understanding of balance control with an inverted pendulum model that fits the center of mass oscillations during walking in different experimental conditions.

INDEX WORDS: Locomotion, Balance control, Center of mass, Split-belt treadmill, Central pattern generator, Neuronal network

MATH MODELING OF INTERLIMB COORDINATION IN CAT LOCOMOTION

by

ELIZAVETA LATASH

A Dissertation Submitted in Partial Fulfillment of the Requirements for the Degree of

Doctor of Philosophy

in the College of Arts and Sciences

Georgia State University

2020

MATH MODELING OF INTERLIMB COORDINATION IN

CAT LOCOMOTION

by

ELIZAVETA LATASH

Committee Chair: Yaroslav Molkov

Committee: Igor Belykh

Vladimir Bondarenko

Gennady Cymbalyuk

Boris Prilutsky

Electronic Version Approved:

Office of Graduate Services

College of Arts and Sciences

Georgia State University

August 2020

DEDICATION

I dedicate my dissertation to my father, Mark Latash for being a wonderful role model in his approach to the world and for teaching me to ask interesting questions. He often quoted his first advisor, Victor Gurfinkel, who said, “There are no uninteresting problems. There are uninteresting ways to deal with any problem.” I also dedicate my dissertation to my father for pathing the path to neuroscience. I am the third generation of the Latash family to study neuroscience, as both he and his father dedicated their lives to this field.

ACKNOWLEDGEMENTS

Above all I would like to acknowledge my primary investigator, Yaroslav Molkov for being such a wonderful mentor throughout my PhD program. He was always insightful, helpful, and pleasant to work with. Yaroslav Molkov inspired me to think critically and objectively. William Barnett was a postdoc in our laboratory and helped guide me through our research. We worked side-by-side on multiple projects. He was a great mentor and brought innovative research concepts and programming methods to our discussions. I would like to acknowledge our committee members, Igor Belykh, Vladimir Bondarenko, Gennady Cymbalyuk and Boris Prilutsky for their guidance and thought provoking questions throughout the proposal and dissertation process. I would like to thank Boris Prilutsky, Illya Rybak, and Alain Frigon for their neuroscience acumen and effort in collaboration on the bodies of research presented in this dissertation.

TABLE OF CONTENTS

LIST OF TABLES

LIST OF FIGURES

LIST OF ABBREVIATIONS

Center of Mass (COM)

Extrapolated Center of Mass (xCOM)

Central Pattern Generator (CPG)

Rhythm Generator (RG)

Flexor (F)

Extensor (E)

Left Hindlimb (LH)

Right Hindlimb (RH)

Left Front Limb (LF)

Right Front Limb (RH)

Slow Hindlimb (SHL)

Fast Hindlimb (FHL)

1 INTRODUCTION

Locomotion is an evolutionary adaptation that allows animals to move in 3-D space. The way that mammalian locomotion is controlled has been studied for generations. It remains unclear how the mammalian locomotor network keeps balance in the face of a changing environment and how the neuronal network that controls locomotion is structured. It is generally accepted that mammalian locomotion is generated by a population of neurons that is located in the spinal cord and are called a central pattern generator (CPG). A CPG provides rhythmic output in the absence of rhythmic input. Variations of the connectivity of the mammalian locomotor CPG have been proposed, but the exact network structure is unclear (1, 2).

During my PhD, my laboratory group and I have made mathematical models that aim to gain understanding of mammalian locomotion and to propose biologically plausible connectivity for the CPG network. Specifically, we made a model of center of mass dynamics based on the equations of motion of the inverted pendulum. The inverted pendulum model is fit to data from a study by Hangue Park titled, “Cutaneous sensory feedback from paw pads affects lateral balance control during split-belt locomotion in the cat” (3). I am the second author of this work due to my contribution in the use of the motion capture platform, VICON to track the locomotion of cats. This work is not included in the presented dissertation because it was already presented in the dissertation of the primary author. We also made a model of neuronal bursting of the cat locomotor CPG and fit the model to cat locomotion data from a work by Alain Frigon titled, “Left–right coordination from simple to extreme conditions during split-belt locomotion in the chronic spinal adult cat” (4) and (5).

Both models, including the one describing center of mass oscillations, use experimental data obtained in cats walked on split-belt treadmills, in which left and right belt speeds may be varied individually (3). In perfect pacing in quadrupeds, front and hind limbs on one side of the body are lifted in unison, while limbs on the other side of the body are on the ground and thus the center of mass oscillates in the frontal plane, such as in bipedal walking. During overground walking, there is a small phase shift between ipsilateral hind- and forelimbs on either side (0.25 – 0.30 of the cycle duration) (6, 7). In cats walking on a treadmill, this phase shift is very small (less or equal to 0.15 of the cycle duration) (6, 8) and thus this gait can be considered pace-like, in which the center of mass oscillates predominantly in the frontal plane as in pacing. We refer to the locomotion of our cats as a pacing gait by this approximation. Recordings of cats pacing were made in various speed conditions with and without cutaneous feedback disruption. Cutaneous feedback disruption is the lack of sensation on the surface of paws due to anesthesia application. The pacing cat is balanced when the center of mass is between the paws, or edges of support. Speed variation is used to study balance control because changing the speed of walking changes the center of mass oscillations. Disrupting sensation of the paws is proposed to disrupt balance and is thus used to study the balance control system.

The recordings made were of cats with spinal input intact. The motor centers of cats with spinal input intact receive input from the brain and process information about the environment for balance control. Varying speed and cutaneous feedback disruption perturb the balance control system and provide a framework for understanding how the motor system keeps balance in a changing environment.

The model of neuronal bursting in the cat locomotor CPG is based on an experimental paradigm in which muscle recordings were made from spinalized cats walking in various speed

conditions (4) and from intact cats walking in various speed conditions (5). Spinalized cats do not receive cortical input to the spinal cord and are not capable of balance control. Studying the locomotion of spinalized cats allows us to study the network that controls locomotor output without balance control function. The behavior of the CPG network is proposed to change with spinal input. Modeling locomotion in spinalized cats allows us to study the behavior of the isolated locomotor CPG network without spinal input. It is generally accepted that each limb is controlled by a separate CPG and that there are interneurons connecting the CPGs for each limb (1, 9). Depending on the exact network architecture, changes in the CPG that corresponds to one limb may change the behavior of the CPG on the opposite side due to interlimb connections. The specific pattern with which cats walk on a split-belt treadmill depends on the interlimb connections in the CPG network architecture. Varying speed unilaterally corresponds to unilateral and bilateral changes in CPG network activity and different interlimb synchronization patterns. Matching the activity in the network to the speed of walking in cats allows us to test biological plausibility of a particular network configuration.

1.1 Specific Aims

1.1.1 *Aim 1:* Investigate the frontal plane dynamics of the center of mass during quadrupedal locomotion on a split-belt treadmill.

In the experiments on which we will base the model of center of mass dynamics, the speed of the right belt increased and the left belt was kept at a constant speed while cats walked on a split-belt treadmill. In a reverse condition, the speed of the left belt was increased.

Cutaneous feedback from front and hind right paws was disrupted in each of the speed conditions. Recordings of the position of the paws and the center of mass were made.

Our model of center of mass dynamics will match the center of mass position normalized to the position of the paws, period, and amplitude of center of mass in cats walking on a split-belt treadmill to the equations of motion for the inverted pendulum. These center of mass parameters have been extracted from center of mass and paw position data that was obtained by the experimentalists during split-belt recordings. These parameters will be obtained for each speed condition, and for conditions with and without cutaneous feedback disruption.

The equations for the inverted pendulum model have been solved analytically by our team. The model uses the position of the center of mass when the right paws begin to lift off of the ground and the position of the center of mass when the left paws are lifted. This model will be fit to the position, amplitude and period parameters using optimization. Using the fitted model, we will be able to determine the position of the center of mass at the moment of paw lift on each side of the body, as well as the velocity of the center of mass for each experimental condition.

Hypotheses for Specific Aim 1:

(i) A model based on inverted pendulum dynamics reproduces the center of mass shift due to speed and cutaneous feedback disruption perturbations found in the experimental work of Park *et al*. 2019 (3).
(ii) The period and amplitude of center of mass oscillations changes with speed perturbation, but not with cutaneous feedback disruption.
(iii) The left and right stability thresholds shift by the same amount during cutaneous feedback disruption.
(iv) The lateral stability threshold is greater on the side of the body opposite the slower belt during speed perturbation.

(v) The shift in thresholds for limb lift due to cutaneous feedback disruption is symmetric with respect to speed perturbation. The shift in left and right thresholds for limb lift due to disruption of cutaneous feedback is of the same magnitude when the ratio of left to right split belt speeds is the same.

(vi) The shift in thresholds for limb lift due to cutaneous feedback disruption is reproduced by the pendulum model.

1.1.2 *Aim 2:* Reveal interlimb coordination mechanisms by split-belt locomotion studies.

In the experiments on which we will base the model of neuronal bursting in the locomotor CPG, the speed of the right belt was increased individually while spinalized cats walked on a split-belt treadmill. Recordings from muscles that correspond to flexion and extension of each limb were made. The duration of flexion and extension was determined for each experimental condition. When the speed of the right belt was much higher than the left belt the right paws took multiple steps for each step on the left side.

A CPG network was formulated on the basis of a previously proposed network by Danner *et al.* 2019 (10). This network was simplified by combining connections. We currently have a working model in C++ and in Matlab. We aim to show that the simplified network with a particular connectivity reproduces the duration of flexion and extension observed in the experiments.

The model network consists of two flexor neurons and two extensor neurons that correspond to the control of flexion and extension of two hind limbs. A burst (train of action potentials) of a flexor neuron corresponds to a single flexion of a limb, while a burst of an extensor neuron corresponds to an extension of the limb. An excitatory drive to each flexor increases the rate of bursting and corresponds to increased speed of walking on the split-belt

treadmill. We propose that if our network connectivity is valid, the duration of flexion and extension and the phase relationship between them will correspond to the durations and phases seen in experiment. We also propose to see multiple bursts on one side of the network that correspond to multiple steps on one side of the split-belt treadmill in the experiments.

Hypotheses for Specific Aim 2:

(i) A mathematical model of interacting locomotor central pattern generators that is based on the model of Danner *et al.* 2019 (10) reproduces the experimental findings of Frigon *et al.* 2017 (4). Specifically, the Danner *et al.* 2019 model includes interneurons believed to exist in the locomotor central pattern generator on the basis of experimental and modeling work. The combination of these interneurons is net inhibitory. A reduction of these connections is sufficient to reproduce the findings of Frigon *et al.* 2017.

(ii) An excitatory drive to flexor neuron populations increases bursting rate and reproduces the effect of increasing speed of walking.

(iii) Flexor and extensor neuronal populations are conditional oscillators whose activity regimes depend on the amount of excitatory drive they receive. When the flexor population receives a low drive the flexor half-center bursts at a low frequency, such as in slow walking. In this case, the extensor population receives a relatively high drive and is in tonic mode. With high drive to flexor neurons, the flexor half-center bursts at a high frequency, such as in faster walking. The extensor population then receives a lower drive and begins to burst.

(iv) The decreasing drive to the extensor population that matches increasing drive to flexor population reflects the presence of inhibition of extensor neurons by flexor neurons.

(v) Adopting the mathematical model to the experimental results will elucidate potential neuronal mechanisms of interlimb coordination.

We use mathematical models as a framework to ask questions about the nervous system. In the second chapter, we use the inverted pendulum model to study balance control. The inverted pendulum equations have been used to model balance control in locomotion by defining a condition for stability (11). In our study, the lateral swing of an inverted pendulum swings

models the center of mass oscillations of cats. In the third chapter, we use a model of the rate of voltage change in neurons to study the connectivity of the locomotor CPG network. It is common to simulate neuronal oscillations by the change in voltage over time with a system of ODEs (1, 10, 12) . The change in the phase relationship between cells with varying connectivity strength, parameter values, and drive to the system can be determined in such a system. We gain insight about the structure of the locomotor CPG by matching the phase relationship of cells corresponding to flexion and extension of limbs in such a system to the phase relationship of flexion and extension in cats.

2 FRONTAL PLANE DYNAMICS OF THE CENTER OF MASS DURING QUADRUPEDAL LOCOMOTION ON A SPLIT-BELT TREADMILL

2.1 Introduction

Quadrupedal animals must coordinate the motion of limbs in order to maintain balance. Balance is controlled by keeping the position of the center of mass (COM) between the weight-bearing limbs; e.g. (13). Animals are said to be statically stable when the COM projection is within the edges of support (11, 13). While this may seem trivial for a quadruped standing at rest (14), it becomes more complicated when the animal begins to move. Animals are said to be dynamically stable when the extrapolated center of mass (xCOM) projection is within the edges of support (11). During walking, quadrupedal animals must continuously maintain balance in both the lateral and longitudinal directions. For example, walking cats are statically unstable laterally and dynamically unstable longitudinally during ipsilateral and diagonal double support phases, respectively (15).

The lateral control of balance is particularly important in bipedal locomotion, e.g. in walking ducks (16), penguins (17), non-human primates (18) and humans (19, 20), where the moving animal is only supported by a single limb for most of the walking cycle. During phases of single-limb support, the body may be modeled as an inverted pendulum (21). According to this model, lateral balance is maintained by timely placing the swing limb on the ground to stop the body, falling under the action of gravitational moment, and changing the pivot point of the inverted pendulum and thus the direction of the gravitational moment with each step (21, 22). To plan the timing and position of limb placement, the balance control system must have knowledge of the mechanical state of the walker, i.e. the COM position and velocity with respect to the

boundaries of support (11, 23). This information is likely obtained from the integration of visual, vestibular, proprioceptive and cutaneous afferent signals (24), although the contribution of individual sensory modalities to the integrated sensory input is still uncertain.

Though derived in the context of bipedal locomotion, the inverted pendulum principles could potentially be extended and applied to quadrupedal walking. For example, the kinetic and potential energies of the body in the sagittal plane show out-of-phase changes in the walking cycle of dogs, macaques and rams, resembling the behavior of an inverted pendulum (25, 26). Frontal plane COM motion resembles that of bipeds in long-legged quadrupeds: dogs (27), camels (28), giraffes (29) and alpacas (30), who use a pace-like walking gait, in which the phase difference between the ipsilateral hindlimb and forelimb footfalls approaches zero (31). During pace walking, the animal body is supported mostly by either pair of ipsilateral limbs. Nevertheless, majority of quadrupedal animals during medium-speed walking use a lateral sequence of limbs to support the body with either two or three feet on the ground at all times. For example, in cats walking over-ground at speeds ~0.4–1.0 m/s, the ipsilateral limb phase difference is 0.25–0.30 of the cycle duration (6, 7). During cat treadmill walking, on the other hand, this phase difference is much smaller ≤ 0.15 (6, 8), so the COM frontal plane dynamics of cats walking on a treadmill could be similar to those of bipeds and inverted pendulum.

Indeed, we have demonstrated in cats walking on a treadmill (3) that lateral displacements of the COM and extrapolated COM, xCOM (11), with respect to the borders of support (center of pressure, COP) are strikingly similar to those of humans (22, 32) and thus could potentially be explained by the dynamics of an inverted pendulum. The results of our previous study have also suggested that cats regulate lateral balance by controlling the timing of the ipsilateral double-support phase onset (or the timing of swing onset of the contralateral

forelimb). However, the extent to which frontal plane dynamics of the cat walking on a treadmill can be explained by the inverted pendulum model has not been rigorously investigated.

The goal of this study was to investigate if an inverted pendulum-based model can reproduce major features of the frontal plane COM dynamics of cats walking on a treadmill. The second goal was to use this model to interpret the effects of experimental perturbations of lateral stability. We used two types of perturbations: (i) different speed-ratios of the left and right treadmill belts during split-belt locomotion and (ii) unilateral paw pad anesthesia. Increasing belt-speed asymmetry during split-belt treadmill locomotion leads to reduction of the lateral margins of dynamic stability on the slower side in both humans (33, 34) and cats (3). Cutaneous feedback from the feet has been implicated in regulation of lateral balance in cats (35, 36) and humans (37, 38). Therefore, we expected that compromising cutaneous feedback from paw pads by anesthesia unilaterally would impact lateral balance dynamics. By modeling the cat COM lateral dynamics in the range of these experimental perturbations, we hoped to understand better the mechanisms of balance control in the frontal plane and, in particular, contributions of cutaneous feedback in this control.

2.2 Methods

2.2.1 Experimental Data Collection

All experimental procedures were consistent with the Principles of Laboratory Animal Care (publication of the National Research Council of the National Academies, 8th edition, 2011)

and approved by the Georgia Tech Institutional Animal Care and Use Committee (protocol numbers A100012DO and A100011UV).

Animal subjects and all experimental procedures and conditions were the same as in our previous study (3), so only their brief description is provided here. Four adult female cats with mass ranging from 2.55 to 4.10 kg took part in the experiments. After 3-4 week training with food reward, each cat walked on a split-belt treadmill (Bertec Corporation, Columbus, OH, USA) at four speed combinations of the left and right treadmill belts. In the control condition, cats walked on a treadmill with equal split-belt speeds of 0.4 m/s (speed ratio 1:1). The speed of the right belt was increased by a factor of 1.5 to 0.6 m/s and by 2 times to 0.8 m/s for two additional split-belt speed ratios (0.4 m/s : 0.6 m/s or 1:1.5 and 0.4 m/s : 0.8 m/s or 1:2). In the last speed condition, the speed of the left belt was increased by 2 times to 0.8 m/s, while the right belt was kept at 0.4 m/s (0.8 m/s : 0.4 m/s or 2:1). In each split-belt condition, the cat first walked for 15 s at equal belt speeds of 0.4 m/s; subsequently the speed ratio was changed to a desired value within 1 s, maintained for 60 s, and then returned to the initial equal speed condition within 1 s, and maintained for additional 15 s. The order of the tested split-belt speed conditions was randomized within each animal.

For additional perturbation of lateral balance by compromising cutaneous feedback from paw pads (see Introduction), the same split-belt speed conditions were tested with unilateral paw pad anesthesia on a separate day. The order of testing sessions with and without anesthesia was randomized across animals. Paw anesthesia was administered using lidocaine injections in each pad of the right forepaw and right hindpaw. The anesthesia caused removal of cutaneous sensory feedback from the right paws for about 30 min, during which time the locomotion testing was performed; for details see (3).

During locomotor experiments, 3D coordinates of 28 markers, placed bilaterally on the metatarsophalangeal, ankle, knee and hip joints and the head, were recorded with a 6-camera motion-capture system (Vicon, UK) at a sampling rate of 250 Hz. Recorded marker coordinates (filtered by a 4-th order Butterworth zero-lag filter, cut-off frequency 15 Hz) and 3D mechanical model of the cat body were used to compute the COM coordinates; for details see (7, 39).

2.2.2 Experimental Data Analysis

We used computed COM and paw positions as functions of time to derive relevant parameters of the model. Specifically, we defined the period of lateral COM oscillations (P) as the duration of the cycle, the amplitude of lateral COM oscillations (A_{COM}) as half of the difference between maximum and minimum lateral coordinate of the COM during one cycle, the lateral positions of left and right hindpaws (LH & RH), and the lateral COM position relative to the left hindpaw position normalized to the hindpaw step width (Z_{COM}); see Figure 2.1A. We selected for analysis contiguous 60-s motion recordings of each split-belt condition, removing the first 10 seconds of each recording, during which walking was less regular. This irregularity normally occurred within first 5 seconds after the 1-s speed change from the initial speed ratio of 1:1. We observed no motor adaptation to asymmetric belt speeds in terms of step length, step duration, and duty cycle. That was consistent with a previous report of lack of motor adaptation to prolonged split-belt locomotion in cats (40). Recordings were divided into stride cycles, defined by the moment of right hindpaw placement on the ground. Each parameter was determined in each cycle of each experimental condition and each animal.

Average COM position was calculated for each cycle by taking the average value of the COM coordinates across all time-points within a single cycle. The average COM position for a

subject in one condition was obtained by averaging across all cycles in a single recording. Standard error values were calculated across subjects in a single condition. The equations for the above locomotor parameters are listed below:

$$P = T_{RHon} - T'_{RHon}, \quad (1)$$

$$A_{CoM} = \frac{max_{COM} - min_{COM}}{2}, \quad (2)$$

$$Z_{CoM} = \frac{LH - COM}{LH - RH}, \quad (3)$$

where P is the stride cycle period; T_{RHon} and T'_{RHon} are the times of the current and previous stance onsets of the right hindpaw, respectively; A_{CoM} is the COM oscillation magnitude in the lateral direction; max_{COM} and min_{COM} are the maximum and minimum values of the COM lateral displacement in the cycle; Z_{CoM} is the average normalized lateral COM position; LH and RH are the lateral positions of the left and right hindpaws, respectively (see Fig. 2.1A).

Figure 2.1 **Data processing and modeling notations.**

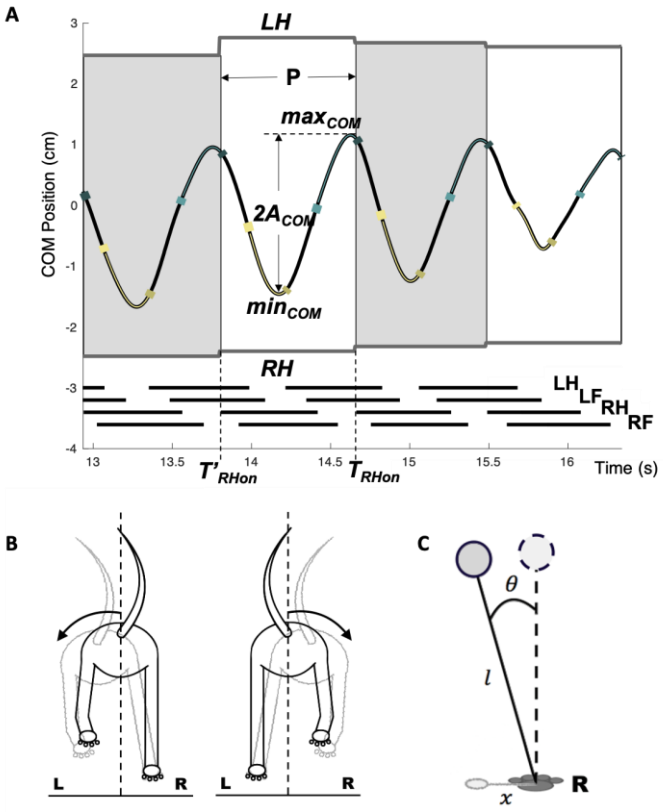

A. Definition of COM kinematic parameters. The oscillating line corresponds to the lateral displacement of the COM during selected strides of treadmill locomotion with symmetric belt speeds (40 cm/s; cat #03, without anesthesia). Positive and negative COM values correspond to displacements in the left and right directions. Square tick marks in the center of mass oscillations show the time of hindpaw lift and placement on the ground for the right hindpaw in turquoise and the left hindpaw in khaki. Positions of the top and bottom sides of each rectangle correspond to the mean lateral position of the left and right hindpaw averaged over the cycle. The height of gray and white rectangles corresponds to the mean hindpaw step width in each cycle. Horizontal thick lines at the bottom indicate the stance period of each limb; left hind (LH), left fore (LF), right hind (RH), and right fore (RF) limbs. The thickness of the rectangles is the step cycle period, P, defined by timing of right hindlimb placements on the ground (T'_{RHon} and T_{RHon}). The amplitude, A_{COM}, is half of the distance between the maximum and minimum COM points in one cycle. **B**. Body oscillations. The direction of the body movement is depicted by arrows. When the left (L) paws are lifted, the body is dragged to the left by the gravitational moment. When the right (R) paws are lifted, the body is dragged to the right. **C.** The inverted pendulum approximation. The inverted pendulum swings at an angle θ from the vertical in the frontal plane. The length of the pendulum is l and the lateral displacement of the COM vertical projection is x.

2.2.3 Model Development

For the stationary cat to remain upright, the COM vertical projection must stay between the borders of support on either side. However, if the COM is moving with some lateral velocity v, this could make the cat dynamically unstable. Which is to say that v must not exceed the value at which the extrapolated center of mass, *xCOM*, crosses the border of support, or the animal will not be able to suppress its lateral motion to prevent the COM from moving beyond the border of support. The extrapolated center of mass is defined as $xCOM = COM + v/\omega$, where $\omega = \sqrt{g/l}$, g is the acceleration due to gravity, and l is the maximum height of the center of mass (11); see Fig. 2.1B, C.

Presume that the cat makes balance control decisions based upon the *xCOM* position in order to maintain dynamic stability. The limb lift-off times on either side would be determined by some position thresholds p_L and p_R of *xCOM* such that p_R defines the transition from the support on both sides (two-side support) to unilateral stance on the right side; p_L defines the transition from the two-side support to unilateral stance on the left side. In this case, the decision-making thresholds would still be determined during the two-side support phases. During these phases, the state of dynamic stability would be defined by the inequalities $p_R < xCOM < p_L$. Given the definition of *xCOM*, we can rewrite these expressions to be $p_R < COM - q/\omega$ and $COM + q/\omega < p_L$ ($q = |v|$) taking into account the direction of COM movement. Based on our previous study we made an assumption that the lateral speed of the COM is roughly constant during and across intervals of support on both sides of the body, which occur during either 3-limb support or diagonal 2-limb support phases; see Fig. 2A and Fig. 8A in (3). Since q is constant, the decision-making thresholds can be formulated for *COM* rather than *xCOM* position as follows:

$$s_R < COM < s_L\ , \qquad (4)$$

where $s_R = p_R + q/\omega$, $s_L = p_L - q/\omega$.

Over the course of a complete stride cycle, the equations of motion that govern the lateral position of COM are determined by the decision-making thresholds s_L and s_R. These thresholds represent the lateral coordinates of the COM at which the cat ipsilateral limbs transition to and from the phases of the two-side support (Phases 1 and 3 in Fig. 2.2) and unilateral swing or contralateral stance (Phases 2 and 4; Fig. 2.2).

Figure 2.2 **Phases of lateral COM displacement in a walking cycle.**

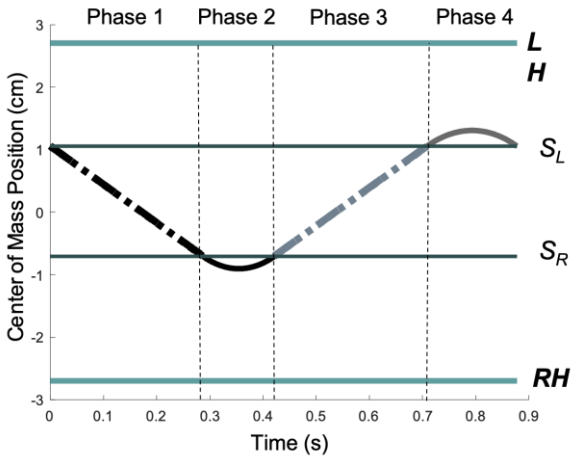

The COM position is shown as a function of time in a walking cycle. Upward and downward directions correspond to displacements to left and right, respectively. Green thick lines at 2.7 cm and -2.7 cm show the average position of left and right hindpaws, labelled as LH and RH, respectively. During Phase 1, the COM moves from left to right from threshold s_L to threshold s_R with constant speed. At threshold s_R the left paws are lifted. During Phase 2, the COM first continues moving right at threshold s_R, but changes direction in mid phase and starts moving leftward to threshold s_R due to the action of the gravitational moment and then it crosses s_R when the left paws are placed back on the ground. In Phase 3, the COM moves from right to left from threshold s_R to threshold s_L at constant speed. At threshold s_L the right paws are lifted. During Phase 4, the COM first continues moving left at threshold s_L, but then changes direction in mid phase and starts moving rightward to threshold s_L due to the action of the gravitational moment.

During Phase 1, the cat is supported by the limbs on both sides of the body, and the dynamics of the lateral COM coordinate x is determined by $dx/dt = -q$ with an initial condition $x(0) = s_L$. Phase 1 lasts until the COM crosses the threshold s_R. Since the COM travels with constant velocity $-q$, the duration of this interval can be written as $T_1 = (s_L - s_R)/q$, and its equation of motion is

$$x(t) = s_L - qt. \tag{5}$$

Then, the cat swings the left limbs as the COM crosses the threshold s_R, transitioning the model into Phase 2.

During Phase 2, the left limbs are in the swing, and the COM accelerates in the leftward direction away from the position of unilateral support on the right side. In this phase, the dynamics of COM is determined by the inverted pendulum equation

$$\frac{d^2x}{dt^2} = \omega^2(x + h), \tag{6}$$

where $-h$ is the coordinate of the right paw. When Phase 2 begins, the model inherits its initial conditions from the previous phase:

$$x(T_1) = s_R, \;\; x'(T_1) = -q. \tag{7}$$

The equation of motion of the COM during Phase 2 is

$$x(t) = -h + (h + s_R)\cosh(\omega(t - T_1)) - \frac{q}{\omega}\sinh(\omega(t - T_1)). \tag{8}$$

The minimum of the COM coordinate is

$$x_{min} = -h + \sqrt{(h + s_R)^2 - \frac{q^2}{\omega^2}}, \tag{9}$$

and the duration of Phase 2 is

$$T_2 = \frac{1}{\omega}\ln\frac{\omega(h+s_R)+q}{\omega(h+s_R)-q}. \tag{10}$$

Phase 2 ends as the COM crosses threshold s_R, entering a phase of dual support (Phase 3).

In Phase 3, the cat once more has support on both left and right sides of the body, and the dynamics is determined by the equation $dx/dt = q$, and its initial condition is $x(T_1 + T_2) = S_R$. The time it takes the COM to traverse the distance between the two decision-making thresholds is $T_3 = (s_L - s_R)/q$, and its equation of motion is

$$x(t) = s_R + q(t - T_1 - T_2). \quad (11)$$

At the end of Phase 3, the right limbs are lifted as the COM crosses the threshold s_L, and the model enters Phase 4.

While the right limbs are in swing phase, the COM accelerates away from the position of support provided by the left limbs:

$$\frac{d^2x}{dt^2} = \omega^2(x - h), \quad (12)$$

where h is the coordinate of the left paw. At the beginning of Phase 4, the initial conditions are:

$$x(T_1 + T_2 + T_3) = s_L \text{ and } x'(T_1 + T_2 + T_3) = q.$$

The equation of motion during Phase 4 is

$$x(t) = h - (h - s_L)\cosh(\omega(t - T_1 - T_2 - T_3)) + \frac{q}{\omega}\sinh(\omega(t - T_1 - T_2 - T_3)). \quad (13)$$

The maximum COM displacement during Phase 4 is

$$x_{max} = h - \sqrt{(h - s_L)^2 - \frac{q^2}{\omega^2}}, \quad (14)$$

and the duration of Phase 4 is

$$T_4 = \frac{1}{\omega}\ln\frac{\omega(h - s_L) + q}{\omega(h - s_L) - q}. \quad (15)$$

In this way, the thresholds s_L and s_R determine the position of COM at which two-side support changes to unilateral support.

Given these expressions, we can analytically compute the quantities $A_{COM}(s_L,s_R,q)$, P(s_L,s_R,q) and $Z_{COM}(s_L,s_R,q)$ for our model as functions of model parameters s_L, s_R, and q. The amplitude of the oscillatory solution is

$$A_{COM}(s_L, s_R, q) = \frac{x_{max}-x_{min}}{2}. \quad (16)$$

and the period of the oscillatory solution is

$$P(s_L, s_R, q) = T_1 + T_2 + T_3 + T_4. \quad (17)$$

The average COM position is defined over cycle as

$$\overline{COM} = \frac{1}{P}\int_0^P x(t)dt. \quad (18)$$

which we normalize to the relative position in the base of support:

$$Z_{COM}(s_L, s_R, q) = \frac{h-\overline{COM}}{2h}, \quad (19)$$

Here, h is the distance from the midline to the support position on either side.

2.2.4 Model Parameter Inference

After processing the experimental data as described above, we obtained average values of the period, amplitude and normalized COM position, P, A, Z_{COM}, and their standard errors $\delta P, \delta A, \delta Z$ for each experimental condition. To find the corresponding values of model parameters we numerically solved the system of equations for s_L, s_R, and q such that the model output in terms of period, amplitude and average COM position exactly matched the experimental measurements: $A_{COM}(s_L, s_R, q) = A$, $P(s_L, s_R, q) = P$, and $Z_{COM}(s_L, s_R, q)$=Z_{COM}. We then computed standard errors for s_L, s_R, and q using Bayesian inference with uniform priors. The posterior probability density function for model parameters ($p.d.f.$) was therefore proportional to the likelihood function which was assumed Gaussian:

$$p.d.f. \sim \exp\left\{-\frac{1}{2}\left(\frac{(A-A(s_L,s_R,q))^2}{\delta A^2} + \frac{(P-P(s_L,s_R,q))^2}{\delta P^2} + \frac{(Z_{COM}-Z_{COM}(s_L,s_R,q))^2}{\delta Z^2}\right)\right\}. \quad (20)$$

The computed values for s_R and s_L were used to define parameters for model interpretation for each experimental condition. The distance between thresholds (DT) was defined as the difference between s_L and s_R. The threshold mean (TM) was the average of s_L and s_R. The change in threshold mean with anesthesia (ΔTM_a) was the difference between TM with and without ipsilateral paw anesthesia in one belt-speed ratio.

2.2.5 Statistics

We used a mixed linear model analysis (IBM SPSS 24, Chicago, IL, USA) to determine the significance of effects of cutaneous feedback and belt-speed ratio on Z_{COM}, P, and A_{COM}. In the analysis, cutaneous feedback and belt-speed ratio were within-subject independent factors. Animals and cycles were random factors. The main effect of independent factors and their interactions were determined at a significance level of 0.05. Pairwise comparisons of significant effects were performed with post-hoc tests using the Bonferroni adjustment.

The significance of cutaneous feedback and belt-speed ratio on model parameters was determined with z-tests. Z-scores were determined for model parameter estimates, s_R, s_L, and q, as well as for quantities depended on these parameters used for model interpretation, DT, TM, ΔTM_a. Pairwise comparisons were performed at the 0.05 significance level.

We visualized the comparison of model trajectories to experimental waveforms by superimposing the COM positions across walking cycles for all subjects in one condition. Each walking cycle of a recording was divided into 100 bins. For each bin the mean and standard error of the COM position were calculated to characterize the average waveform and its distribution

for each experimental condition. Then, a chi-square test was used to evaluate goodness-of-fit of the model.

2.3 Results

2.3.1 Model Validation

Lateral COM displacements as simulated by the inverted pendulum were quantitatively similar to the mean COM displacements in different experimental conditions: belt-speed ratios 1:1, 1:1.5, and 1:2 with and without unilateral paw anesthesia (RMSE < 0.01 cm, see Figure 2.3). See supplementary Tables 1 and 2 for RMSE values and chi-squared test results for each condition.

Figure 2.3 **Comparison of model lateral displacements with the mean cat COM displacements in different experimental conditions.**

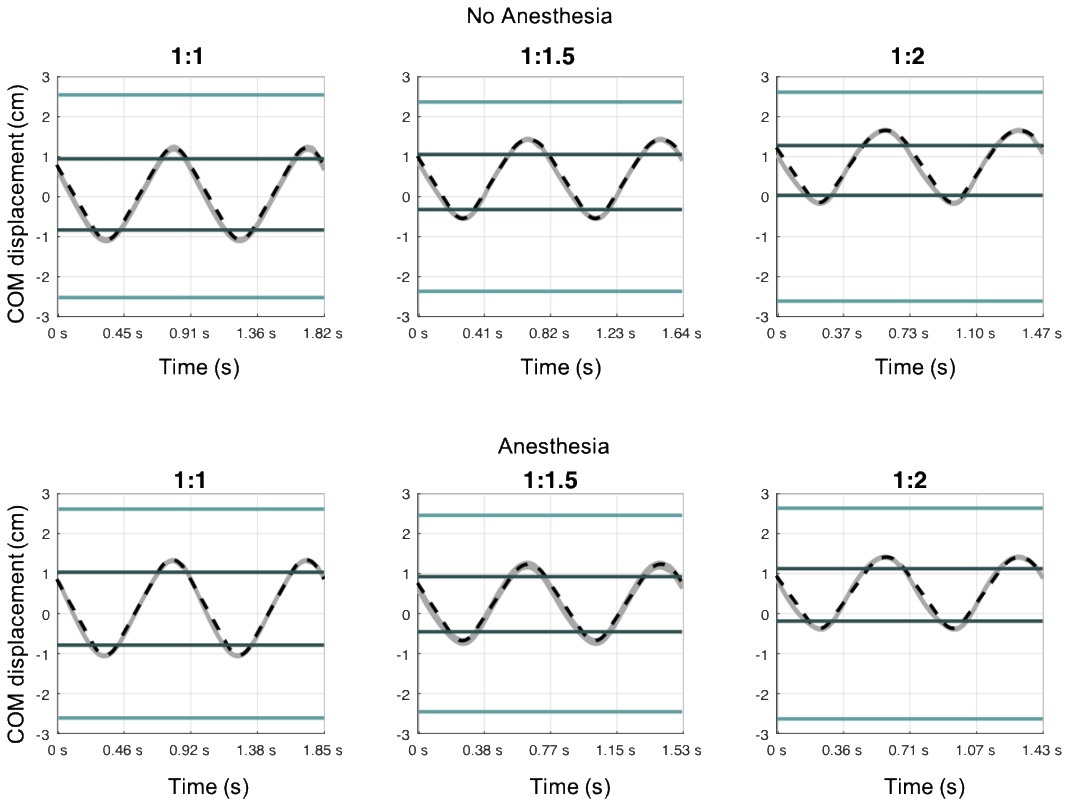

The model (black dashed lines) and experimental (continuous gray lines) displacements are shown for three belt-speed ratios 1:1, 1:1.5 and 1:2 for intact paws (top row) and unilateral paw anesthesia (bottom row). The experimental traces are the means computed across all cycles and cats; the thickness of the gray lines represents ±SE. The dark gray horizontal lines are estimated lateral stability thresholds s_R (top) and s_L (bottom). The mean position of left and right limbs are shown in light blue. The total duration of each plot corresponds to two full cycle periods. All traces start at the onset of the unilateral right-limb support.

Figure 2.4 **Mean normalized lateral COM position Z_{COM} in the cycle, COM oscillation amplitude A_{COM} and stride cycle period P as function of belt-speed ratio and anesthesia.**

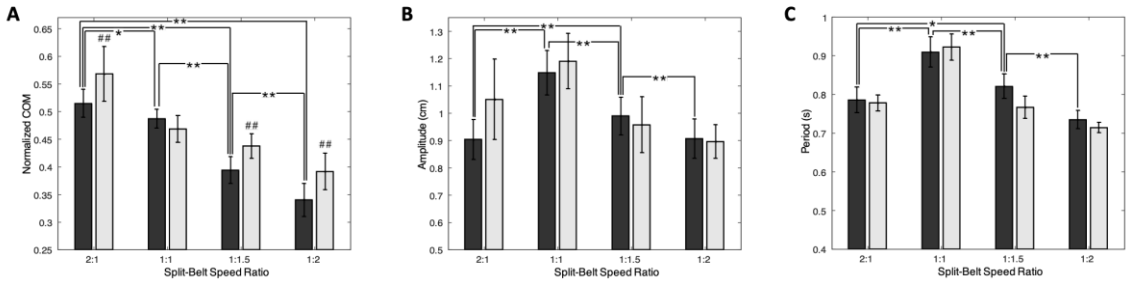

Mean (±SE) were computed over all cats for each experimental condition. In each panel, an experimental measure is shown for split-belt speed ratios 2:1, 1:1, 1:1.5 and 1:2. Dark gray bars show results for intact paws; light gray bars show results for anesthetized right paws. Stars depict significant effects of the speed ratios (single star $p<0.05$, double star $p<0.01$); hashtags (#) depict significant effects of the unilateral anesthesia (# $p<0.05$, ## $p<0.01$). **A**. The COM position normalized to hindpaw step width, Z_{COM}. **B**. COM oscillation amplitude, A_{COM}. **C**. The cycle period, P.

2.3.2 Change in Center of Mass Position with Increasing Right Belt Speed and Unilateral Anesthesia

The COM exhibited a left-right oscillatory motion during treadmill locomotion (Figs. 2.1, 2.3). Experimental COM oscillatory motion parameters, A_{COM}, P, and Z_{COM} , characterized the frontal plane COM dynamics. Z_{COM}, the lateral COM position averaged over the cycle shifted to the left (decreased, see eq. 3) as the belt-speed ratio increased from 1:1 to 1:5 ($p < 0.05$) and from 1:1.5 to 1:2 ($p<0.05$; Fig. 2.4A). At speed ratio 2:1 (at which the left and right belts moved at 0.8 m/s and 0.4 m/s, respectively), Z_{COM} showed a significant right shift compared to speed ratio 1:1. In trials with anesthesia applied to the right paws, Z_{COM} shifted significantly to the right (the values increased; $p<0.05$) for the belt-speed ratios 1:1.5, 1:2 and 2:1, but not for 1:1 (Fig. 2.4A). See supplementary Tables 3 and 4 for all pairwise comparisons of Z_{COM}.

The amplitude of COM oscillations A_{COM} was also found to vary with the speed-belt ratio (Fig. 2.4B). A_{COM} decreased significantly as the belt-speed ratio increased from 1:1 to 1:1.5, to 1:2, and to 2:1, as well as from 1:1.5 to 1:2 and to 2:1 ($p < 0.05$). No significant change in amplitude of oscillations was found between speed ratios 1:2 and the 2:1 ($p = 1.00$). A_{COM} did not change significantly in response to unilateral anesthesia ($p = 0.990$).

Stride cycle period, P, depended on the belt-speed ratio (Fig. 2.4C). The step cycle period decreased from belt speed ratio 1:1 to 1:1.5, to 1:2, and to 2:1, as well as from ratio 1:1.5 to 1:2 and to 2:1 ($p < 0.05$). No significant difference in P was found between speed ratios 1:2 and the 2:1 ($p = 0.082$). Unilateral anesthesia did not induce a significant change in P ($p = 0.077$). See supplementary tables 5 and 6 for all pairwise comparisons of P and supplementary tables 7 and 8 for all pairwise comparisons of A_{COM}.

2.3.3 Changes in Stability Thresholds with Increasing Right Belt Speed and Unilateral Anesthesia

The changes in model parameters were qualitatively similar to the mean experimental COM motion parameters in different experimental conditions: belt-speed ratios 1:1, 1:1.5, 1:2 and 2:1 with and without unilateral paw anesthesia (Fig. 2.3).

We observed a significant left shift of the estimated threshold for initiation of the left ipsilateral support, s_L, with changing the belt-speed ratio from 1:1 to 1:2, from 1:1.5 to 1:2, and from 2:1 to 1:1, to 1:1.5 and to 1:2 for the unanesthetized conditions ($p < 0.05$; Fig. 2.5A). The threshold for initiation of the right ipsilateral support, s_R, also shifted to the left with a change in speed ratio from 1:1 to 1:1.5 and to 1:2, from 1:1.5 to 1:2, and from 2:1 to 1:1.5 and to 1:2 ($p < 0.05$; Fig. 2.5A). There was also a much greater change of threshold s_R than s_L between speed

ratios 1:1 through 1:2, i.e. from -0.835 cm to 0.017 cm for s_R and from 0.931 cm to 1.266 cm for s_L. Anesthesia of the right paws caused a significant right shift of threshold s_L at speed ratios 1:1.5 and 1:2, and of threshold s_R at speed ratios 1:2 and 2:1 ($p < 0.05$; Fig. 2.5A).

Figure 2.5 **Estimated thresholds for initiation of ipsilateral double support phases, s_L and s_R, and model velocity parameter q as function of belt-speed ratio and anesthesia.**

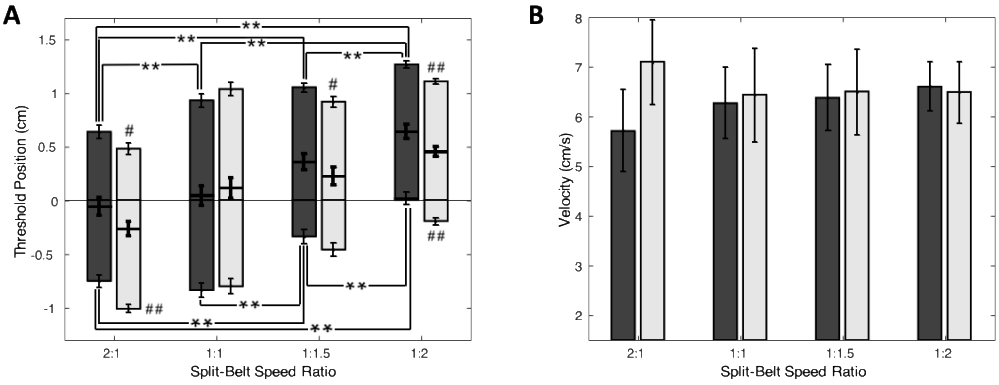

A. Mean thresholds s_L (upper sides of bars) and s_R (lower sides of bars). The average (±SE) of the two thresholds is shown in the middle of each bar. **B**. Model velocity parameter q. Means (±SE) were computed using Bayesian inference for each experimental condition. In each panel, a model parameter is shown for split-belt speed ratios 2:1, 1:1, 1:1.5 and 1:2. Dark gray bars show results for intact paws; light gray bars show results for anesthetized right paws. Stars depict significant effects of the speed ratios (single star $p<0.05$, double star $p<0.01$); hashtags (#) depict significant effects of the unilateral anesthesia (# $p<0.05$, ## $p<0.01$).

We did not detect significant changes in the model velocity parameter q with changes in speed ratio or paw anesthesia conditions ($p > 0.05$; Fig. 2.5B).

Since s_L and s_R depended differently on changes in the right-side belt speed, we quantified the net change in the COM dynamics by the threshold mean—the average of s_L and s_R at a given belt speed ratio and by the distance between thresholds—the difference of s_L and s_R at a given belt speed ratio (Fig. 2.6). The threshold mean significantly increased—indicating a shift to the left side—with a change in belt speed ratio when comparing 1:1 to 1:1.5 and to 1:2 belt speed ratios, as well as in the 1:1.5 to 1:2 and 2:1 belt speed ratio comparison ($p< 0.05$; Fig. 2.6A). The threshold mean significantly decreased with a change in belt speed ratio when comparing the 1:2 to the reverse 2:1 belt speed ratio ($p < 0.05$). The application of anesthesia to right-side paws significantly decreased the threshold mean at the 1:2 belt speed ratio, indicating a shift in the threshold mean towards the right side of the cat. However, when we considered the change in threshold mean in response to anesthesia application across different speed ratios, we did not find significant differences among 2:1, 1:1.5 and 1:2 ratios ($p > 0.05$; Fig. 2.6B). The distance between thresholds did not significantly change with belt speed, except for in the 1:1 to 1:2 belt speed ratio comparison. The distance between thresholds did not change significantly with application of anesthesia to the right paws ($p > 0.05$; Fig. 2.6C). See supplementary tables 9 through 19 for pairwise comparisons of model parameters.

Figure 2.6 **Estimated mean of thresholds s_L and s_R (±SE), the change in threshold mean with anesthesia, and the distance between thresholds as functions of belt-speed ratio.**

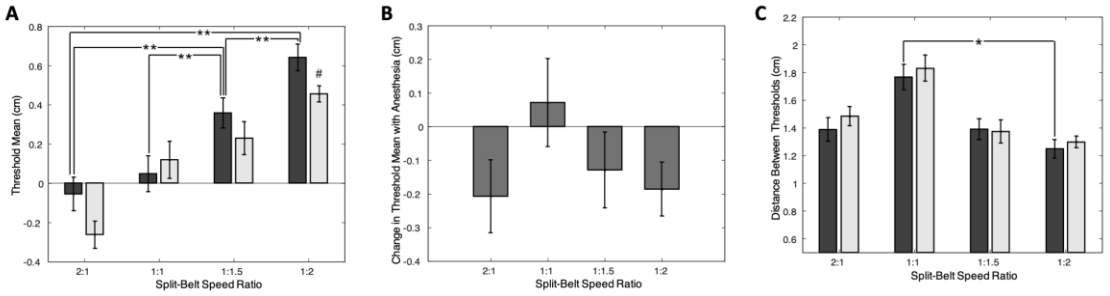

A. The threshold mean (the average of thresholds s_L and s_R). **B**. The change in the threshold mean with the application of anesthesia. **C**. The distance between thresholds s_L and s_R. Means (±SE) were computed using Bayesian inference for each experimental condition. In each panel, a model parameter is shown for split-belt speed ratios 2:1, 1:1, 1:1.5 and 1:2. Dark gray bars show results for intact paws; light gray bars show results for anesthetized right paws. Stars (*) depict significant effects of the speed ratio (* p<0.05, ** p<0.01); hashtags (#) depict significant effects of the unilateral anesthesia (# p<0.05, ## p<0.01).

2.3.4 Effect of Anesthesia is Independent of the Sign of Speed Difference

We found that the change in threshold mean due to anesthesia in terms of its magnitude and direction was not statistically different across speed ratios of 2:1, 1:1.5 and 2:1 (Fig. 2.6B). To explore this further, we compared the changes in both thresholds s_L and s_R due to right-side paw anesthesia for speed ratios 2:1 and 1:2.

The change in the two thresholds due to anesthesia (Δs_L and Δs_R) was found to increase in magnitude with changes in belt-speed ratio from 1:1 to 1:2 and 2:1 ($p < 0.05$). Additionally, the unilateral application of anesthesia to the right side shifted the COM towards the anesthetized side regardless of the speed-belt ratio of 1:2 or 2:1 (Fig. 2.7). There was no significant difference between changes in the thresholds for the two speed ratios ($p > 0.05$).

Figure 2.7 **Effect of anesthesia is independent of the sign of speed difference.**

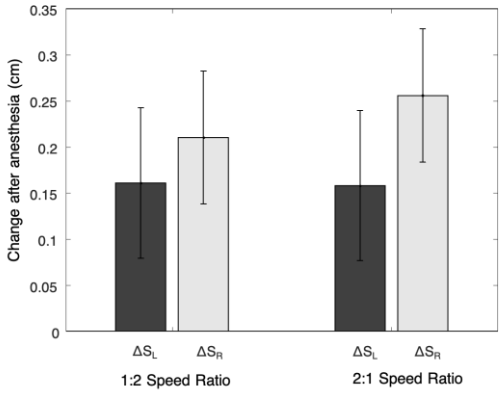

The change in thresholds s_L and s_R due to cutaneous anesthesia applied to right paws for opposite split-belt speed ratios. Comparison shows no significant difference between the changes in thresholds s_L and s_R ($p>0.05$) due to anesthesia for 1:2 and 2:1 speed ratios.

2.4 Discussion

The inverted pendulum-based model closely reproduced the experimentally measured COM lateral oscillations of cats walking on a split-belt treadmill with different belt speed ratios and with intact and unilaterally anesthetized paws (Fig. 2.3). These results support the hypothesis that COM frontal plane dynamics of cats walking on a treadmill can be described by an inverted pendulum model.

We also tested the effect of varying belt speed ratios on COM lateral position and on lateral stability margins. As demonstrated in this (Figs. 2.3, 2.4A and 2.5A) and other recent studies in cats (3) and humans (33, 34), the COM and xCOM shift towards the slower moving split-belt. We found that with a progressive change in belt speed ratio, the increase of the lateral

stability margins on the faster moving side is much greater than the decrease of the stability margins on the slower side (Fig. 2.5A). Thus, the belt speed difference affected the lateral stability margins on the faster and slower sides asymmetrically. The same asymmetric changes in margins of stability have been reported for human split-belt walking in (33) (see their Fig. 2a). The authors have demonstrated (see also (22)) that these results are expected from the dynamics of an inverted pendulum model. In particular, the model predicts an inverse relationship between the duration of the unilateral support phase and the margin of stability on that side. Assuming that the unilateral support phase on the faster moving side of the treadmill is shorter, and therefore the stability margin is greater, the cycle-averaged *xCOM* should shift away from the faster moving leg. On the other hand, humans and presumably cats can voluntarily choose different margins of stability, but prefer to shift COM towards a slower belt. It is likely, therefore, that other factors besides the inverse pendulum dynamics can also affect the asymmetric margins of stability during split-belt walking. One such factor could be energy expenditure, see e.g. (41).

The similarity of experimental and modeling results obtained in humans and cats walking on a split-belt treadmill suggests that there are common mechanisms of lateral balance control in these species. There are, however, some differences. In cats walking on a tied-belt and split-belt treadmill, there is a rather long phase a two-side support (3, 5, 6); see also Figs. 2.1A and 2.2. In contrast, the human double support phase is relatively short and justifiably neglected in inverted pendulum models of frontal plane walking dynamics (22, 33). The difference in the two-side support duration between cats and humans could potentially explain the lack of motor adaptation to asymmetric split-belt speeds in cats (40) as opposed to humans (42).

Using the inverted pendulum-based model, we also inferred the effect of anesthesia application to right paws on model parameters, i.e. lateral stability thresholds. We found that both left and right stability thresholds undergo a symmetric shift towards the anesthetized side regardless of the direction of belt speed difference (Figs. 2.6B and 2.7). As we explain next, these findings suggest that the central nervous system might use cutaneous feedback from paw pads to determine COM position with respects to the paws. Local anesthetic injections in the foot sole effectively diminish cutaneous sensory feedback, resulting in reduced sensation of pressure (43, 44). This might result in a false perception of unloading the paws on the anesthetized side and thus a shift of body weight and COM position towards the contralateral side. Therefore, the animal may attempt to restore the body weight distribution between the left and right limbs by shifting the lateral stability thresholds on both sides of the body, such that perception of body weight distribution is even on the left and right paws. Thus, anesthesia might alter sensory information used to estimate the position of the COM vertical projection within the borders of support. This inference suggests the potential importance of cutaneous feedback from paw pads in the balance control system, or, more specifically, the potential role of the nervous system in setting the lateral stability thresholds during locomotion.

It is possible to derive the relationship between the relative COM shift during unilateral paw anesthesia and the shift in the perception threshold. Let us assume that a reduced cutaneous feedback from ipsilateral paws shifts a perceived COM location in the lateral direction. A COM compensatory shift to restore the pre-anesthesia pressure distribution among the paws should be equal and opposite to the perceived COM shift. Thus, we can use the experimentally measured anesthesia-evoked COM shift to define the extent of the cutaneous feedback reduction by

anesthesia of the ipsilateral paw pads. The relationship between the perceived COM shift and the cutaneous feedback reduction can be derived as described below.

If we neglect relatively small vertical accelerations of the body caused by limb extensions during walking in the cat, i.e. ~2 m/s^2 (~20% of acceleration of gravity; see Fig. 3 in (45)), the sum of the vertical forces applied to the left and right paws from the ground is equal and opposite to *mg*.

$$F_L + F_R = mg, \tag{21}$$

where *m* is the cat's mass and *g* is gravitational acceleration. Since the net rotation of the cat in the frontal plane during the whole walking cycle is zero, the net resultant moment of all forces acting on cat in the frontal plane with respect to the COM must be zero in accordance with conservation of angular momentum. Then, assuming negligibly small ground reaction forces in the medial-lateral direction (15), the resultant moment with respect to the COM in the frontal plane is:

$$0 = F_L(x + h) + F_R(x - h). \tag{22}$$

After solving for *x*, i.e. the COM position between the left (*h*) and right (-*h*) paws, we obtain

$$x = \frac{F_R - F_L}{F_L + F_R}\, h$$

We define F_R' as the perceived load on ipsilateral paws after anesthesia, where $F_R' < F_R$.

$$F_R' = F_R(1 - \delta). \tag{23}$$

Here, δ is a parameter that ranges from 0 to 1 and which represents the percent reduction in load perception. The perceived COM position is defined as x':

$$x' = \frac{F_R' - F_L}{F_L + F_R'}\, h = \frac{F_R(1-\delta) - F_L}{F_L + F_R(1-\delta)}\, h. \tag{24}$$

Therefore, for small δ, the difference between the perceived and actual COM positions $\Delta x = x' - x$ can be approximately found as $\Delta x \approx -h\delta/2$. This bias in perception will lead to the apparent shift of the stability thresholds in the opposite direction: $\Delta s = -\Delta x \approx h\delta/2$. Thus, the contribution of cutaneous receptors to the load perception can be estimates as

$$\delta \approx 2\Delta s/h. \quad (25)$$

Based on our inferences, the stability thresholds were shifted by anesthesia by approximately 0.2 cm (Figs. 2.6B and 2.7) with the half distance between the paws of approximately 2.5 cm (Fig. 2.3), which suggests that cutaneous anesthesia reduced the perception of the force by approximately 16%. This value appears rather small considering that that paw pad anesthesia completely eliminated withdrawal response to pinpricks in our experiments (3). The relatively small reduction in perception of limb load after elimination of touch and pain sensation in paw pads suggests a substantial contribution to load perception from other load sensitive mechanoreceptors located throughout the limb including those responsible for osseoperception (46).

We found that the effect of anesthesia may depend on the magnitude of speed ratio as the shift of the relative COM position and of lateral stability thresholds with anesthesia perturbation was not significant in the 1:1 belt-speed condition, but reached significance at higher belt-speed ratios (Fig. 2.5A). The stronger effect of paw anesthesia with increasing belt speed asymmetry is consistent with previous reports that bilateral removal of cutaneous feedback from cat hindpaws causes greater locomotor deficits in more demanding tasks (i.e., slope and horizontal ladder walking, walking with lateral perturbations) than in normal overground or tied-belt treadmill walking (36, 47). A possible interpretation of our results is that the balance control system's reliance on cutaneous feedback from the paws increases in unusual circumstances and more

demanding tasks such as a large belt-speed difference. Still, during normal cat walking, bilateral removal of hindpaw cutaneous feedback leads to modest changes in locomotor mechanics – lowering the pelvis, shortening step length and increasing the medial-lateral forces exerted by hindlimbs on the ground (36, 47). This indicates that cutaneous feedback from paws plays a role in lateral balance control. Removal of cutaneous feedback from feet in humans also affects lateral balance control (37, 38). Exact mechanisms by which cutaneous feedback from feet contribute to lateral balance control require additional studies. Cutaneous sensory input from various mechanoreceptors in the feet (48, 49) is integrated at different levels of the nervous system from the spinal cord to somatosensory cortex (48). Several studies of locomotion and standing in reduced animal preparations – decerebrate cats and rabbits, have demonstrated that mechanisms of automatic postural corrective responses to lateral body perturbations reside in the spinal cord, brainstem and cerebellum and that somatosensory feedback from the body limbs and trunk is sufficient for initiation and scaling the corrective responses (50, 51).

In conclusion, this study demonstrated that lateral dynamics of cat COM during tied-belt and split-belt treadmill walking can be accurately described by augmenting the inverted pendulum model with the two-side support phase. We found that with increasing asymmetry in belt speeds, margins of dynamic stability on the faster and slower sides change asymmetrically. These results closely resemble the lateral COM dynamics during human walking, suggesting that the cat may be a suitable animal model to study neural mechanisms of lateral balance control during locomotion. In the present study, we obtained initial insights into a possible role of cutaneous feedback from paw pads. In particular, we demonstrated that unilateral removal of paw cutaneous feedback leads to a compensatory COM shift towards the anesthetized side, but only in locomotor conditions with asymmetric belt speeds. In future studies, we plan to use

similar experimental and modeling approaches to study effects of other sensory inputs on dynamic stability in the frontal and sagittal planes in walking cats.

2.5 Supplementary Tables

Condition	**RMSE** (cm)
SR 1:1	0.0007
SR 1:1+	0.0014
SR 1:1.5	0.0010
SR 1:1.5+	0.0058
SR 1:2	0.0018
SR 1:2+	0.0017

Table 2.1 Root mean squared error (RMSE) between experimental and modeled COM displacement computed across 100 data points in the cycle of different experimental conditions. SR is split-belt speed ratio; + depicts conditions with right paw anesthesia.

Condition	$\boldsymbol{\chi^2}$
SR 1:1	p = 1.0000
SR 1:1+	p = 0.9881
SR 1:1.5	p = 1.0000
SR 1:1.5+	p = 0.9459
SR 1:2	p = 0.9908
SR 1:2+	p = 0.8169

Table 2.2 Results of chi-squared test for the model fit results presented in Table 2. SR is split-belt speed ratio; + depicts conditions with right paw anesthesia.

SR	**1:1**	**1:1.5**	**1:2**
1:1.5	**$p < 0.001$**		
1:2	**$p < 0.001$**	**$p < 0.001$**	
2:1	**$p = 0.034$**	**$p < 0.001$**	**$p<0.001$**

Table 2.3 Significance of pairwise comparisons of effects of split-belt speed ratios (SR) on the normalized COM position (Z_{CoM}). Overall effect of speed ratio on Z_{CoM} was significant ($F_{3,826}$ = 99.200, $p < 0.001$).

Conditions	**Significance**
SR 1:1 vs 1:1+	$F_{1,825} = 0.711$, $p = 0.399$
SR 1:1.5 vs 1:1.5+	$F_{1,827} = 8.077$, **$p = 0.005$**
SR 1:2 vs 1:2+	$F_{1,826} = 26.881$, **$p < 0.001$**
SR 2:1 vs 2:1+	$F_{1,827} = 26.973$, **$p < 0.001$**

2.4a

Conditions	**Significance**
Overall vs Overall+	$t_{826} = -5.185$, **$p < 0.001$**

2.4b

Table 2.4 (a) Significance of pairwise comparisons of effects of anesthesia on the normalized COM position (Z_{CoM}) in different experimental conditions. SR is split-belt speed ratio; + depicts conditions with right paw anesthesia. (b) Overall effect of anesthesia on the normalized COM position (Z_{CoM}) during split-belt treadmill walking. + depicts right paw anesthesia.

SR	**1:1**	**1:1.5**	**1:2**
1:1.5	**$p<0.001$**		
1:2	**$p<0.001$**	**$p<0.001$**	
2:1	**$p<0.001$**	**$p=0.026$**	$p=0.082$

Table 2.5 Significance of pairwise comparisons of effects of split-belt speed ratios (SR) on the period (P) of COM oscillations. Overall effect of speed ratio on P was significant ($F_{3,826}$ = 48.730, $p < 0.001$).

Conditions	Significance
SR 1:1 vs 1:1+	$F_{1,825} = 0.003$, p = 0.956
SR 1:1.5 vs 1:1.5+	$F_{1,826} = 13.474$, **p < 0.001**
SR 1:2 vs 1:2+	$F_{1,826} = 3.130$, p = 0.077
SR 2:1 vs 2:1+	$F_{1,827} = 0.031$, p = 0.861

2.6a

Conditions	Significance
Overall vs Overall+	$t_{826} = 1.769$, p = 0.077

2.6b

Table 2.6 (a) Significance of pairwise comparisons of effects of anesthesia on the period (*P*) of COM oscillations in different experimental conditions. SR is split-belt speed ratio; + depicts conditions with right paw anesthesia. (b) Overall effect of anesthesia on the period (*P*) of COM oscillations during split-belt treadmill walking. + depicts right paw anesthesia.

SR	1:1	1:1.5	1:2
1:1.5	**p=0.010**		
1:2	**p<0.001**	**p=0.004**	
2:1	**p<0.001**	**p<0.001**	p=1.000

Table 2.7 Significance of pairwise comparisons of effects of split-belt speed ratios (SR) on the amplitude of COM oscillations (A_{CoM}). Overall effect of speed ratio on A_{CoM} was significant ($F_{3,825} = 42.755$, p < 0.001).

Conditions	Significance
SR 1:1 vs 1:1+	$F_{1,825}$ = 0.165, p = 0.685
SR 1:1.5 vs 1:1.5+	$F_{1,825}$ = 9.453, **p = 0.002**
SR 1:2 vs 1:2+	$F_{1,825}$ = 0.000, p = 0.990
SR 2:1 vs 2:1+	$F_{1,826}$ = 5.746, **p = 0.017**

2.8a

Conditions	Significance
Overall vs Overall+	t_{826} = -0.013, p = 0.990

2.8b

Table 2.8 (a) Significance of pairwise comparisons of effects of anesthesia on the amplitude of COM oscillations (A_{CoM}). SR is split-belt speed ratio; + depicts conditions with right paw anesthesia. (b) Overall effect of anesthesia on the amplitude of COM oscillations (A_{CoM}) during split-belt treadmill walking. + depicts right paw anesthesia.

SR	1:1	1:1.5	1:2
1:1.5	Z=1.622, p=0.105		
1:2	Z=4.674, **p<0.001**	Z=3.929, **p<0.001**	
2:1	Z=3.354, **p<0.001**	Z=5.632, **p<0.001**	Z=8.970, **p<0.001**

Table 2.9 Significance of pairwise comparisons of effects of split-belt speed ratios (SR) on threshold s_L. Z indicates z-score for a between-groups z-test.

Conditions	Significance
SR 1:1 vs 1:1+	Z=1.159, p=0.247
SR 1:1.5 vs 1:1.5+	Z=2.024, **p=0.043**
SR 1:2 vs 1:2+	Z=3.77, **p<0.001**
SR 2:1 vs 2:1+	Z=1.941, **p=0.050**

Table 2.10 Significance of pairwise comparisons of effects of anesthesia on threshold s_L. Z indicates z-score for a between-groups z-test. SR is split-belt speed ratio; + depicts conditions with right paw anesthesia.

SR	**1:1**	**1:1.5**	**1:2**
1:1.5	Z=5.475, **p<0.001**		
1:2	Z=9.742, **p<0.001**	Z=4.108 **p<0.001**	
2:1	Z=0.974, p=0.330	Z=4.769, **p<0.001**	Z=9.257, **p<0.001**

Table 2.11 Significance of pairwise comparisons of effects of split-belt speed ratios (SR) on threshold s_R. Z indicates z-score for a between-groups z-test.

Conditions	**Significance**
SR 1:1 vs 1:1+	Z=0.405, p=0.686
SR 1:1.5 vs 1:1.5+	Z=1.400, p=0.180
SR 1:2 vs 1:2+	Z=3.127, **p=0.002**
SR 2:1 vs 2:1+	Z=3.541, **p=<0.001**

Table 2.12 Significance of pairwise comparisons of effects of anesthesia on threshold s_R. Z indicates z-score for a between-groups z-test. SR is split-belt speed ratio; + depicts conditions with right paw anesthesia.

SR	**1:1**	**1:1.5**	**1:2**
1:1.5	Z=0.111, p=0.911		
1:2	Z=0.378, p=0.705	Z=0.268, p=0.789	
2:1	Z=0.511, p=0.610	Z=0.633, p=0.527	Z=0.931, p=0.352

Table 2.13 Significance of pairwise comparisons of effects of split-belt speed ratios (SR) on the COM speed q. Z indicates z-score for a between-groups z-test.

Conditions	Significance
SR 1:1 vs 1:1+	Z=0.129, p=0.897
SR 1:1.5 vs 1:1.5+	Z=0.101, p=0.920
SR 1:2 vs 1:2+	Z=0.155, p=0.877
SR 2:1 vs 2:1+	Z=1.168, p=0.243

Table 2.14 Significance of pairwise comparisons of effects of anesthesia on the COM speed q. Z indicates z-score for a between-groups z-test. SR is split-belt speed ratio; + depicts conditions with right paw anesthesia.

SR	1:1	1:1.5	1:2
1:1.5	Z=2.626, **p=0.009**		
1:2	Z=5.249, **p<0.001**	Z=2.785, **p=0.005**	
2:1	Z=0.838, p=0.402	Z=3.641, **p<0.001**	Z=6.430, **p<0.001**

Table 2.15 Significance of pairwise comparisons of effects of split-belt speed ratios (SR) on the threshold mean (*TM*). Z indicates z-score for a between-groups z-test.

Conditions	Significance
SR 1:1 vs 1:1+	Z=0.542, p=0.587
SR 1:1.5 vs 1:1.5+	Z=1.143, p=0.253
SR 1:2 vs 1:2+	Z=2.331, **p=0.020**
SR 2:1 vs 2:1+	Z=1.901, p=0.057

Table 2.16 Significance of pairwise comparisons of effects of anesthesia on the threshold mean (*TM*). Z indicates z-score for a between-groups z-test. SR is split-belt speed ratio; + depicts conditions with right paw anesthesia.

SR	1:1	1:1.5	1:2
1:1.5	Z=1.157, p=0.247		
1:2	Z=1.675, p=0.094	Z=0.413, p=0.680	
2:1	Z=1.633, p=0.103	Z=0.500, p=0.617	Z=0.158, p=0.875

Table 2.17 Significance of pairwise comparisons of effects of split-belt speed ratios (SR) on the change in threshold mean due to anesthesia (ΔTM_a). Z indicates z-score for a between-groups z-test.

SR	1:1	1:1.5	1:2
1:1.5	Z=1.592, p=0.111		
1:2	Z=2.287, **p=0.022**	Z=0.693, p=0.488	
2:1	Z=1.528, p=0.127	Z=0.012, p=0.991	Z=0.638, p=0.523

Table 2.18 Significance of pairwise comparisons of effects of split-belt speed ratios (SR) on the difference between left and right thresholds (*DT*). Z indicates z-score for a between-groups z-test.

Conditions	Significance
SR 1:1 vs 1:1+	(Z=0.246, p=0.806)
SR 1:1.5 vs 1:1.5+	(Z=0.071, p=0.944)
SR 1:2 vs 1:2+	(Z=0.310, p=0.757)
SR 2:1 vs 2:1+	(Z=0.449, p=0.653)

Table 2.19 Significance of pairwise comparisons of effects of anesthesia on the difference between left and right thresholds (*DT*). Z indicates z-score for a between-groups z-test. SR is split-belt speed ratio; + depicts conditions with right paw anesthesia.

Conditions	**Statistics**
Δs_{La} at SR 1:1 vs 1:2	(Z=2.674, **p=0.007**)
Δs_{La} at SR 1:1 vs 2:1	(Z=2.165, **p=0.030**)
Δs_{Ra} at SR 1:1 vs 1:2	(Z=2.127, **p=0.033**)
Δs_{Ra} at SR 1:1 vs 2:1	(Z=2.454, **p=0.014**)

Table 2.20 Significance of pairwise comparisons of effects of split-belt speed ratios (SR) on the shift in thresholds s_L and s_R with anesthesia. Z indicates z-score for a between-groups z-test.

Conditions	Δs_{La}	Δs_{Ra}
SR 2:1	0.158 ± 0.082	0.256 ± 0.072
SR 1:2	0.161 ± 0.082	0.211 ± 0.072

Table 2.21 The average value ± standard error for the shift in thresholds s_L and s_R with anesthesia are shown for different speed ratios (SR).

Conditions	**Statistics**
Δs_{La} at SR 2:1 vs 1:2	Z=0.025, p=0.980
Δs_{Ra} at SR 2:1 vs 1:2	Z=0.445, p=0.656

Table 2.22 Significance of pairwise comparisons of effects of split-belt speed ratios (SR) on the shift in thresholds s_L and s_R with anesthesia. Z indicates z-score for a between-groups z-test.

3 ON THE ORGANIZATION OF THE LOCOMOTOR CPG: INSIGHTS FROM SYMMETRIC AND ASYMMETRIC (SPLIT-BELT) LOCMOTION AND MATHEMATICAL MODELING

3.1 Introduction

It is commonly accepted that the spinal central pattern generator (CPG) that controls locomotion includes separate rhythm generators (RGs) that each control a single limb and interact with each other via multiple commissural and homolateral circuits. These circuits set up phase relationships between the RGs and thus coordinate limb movements and locomotor gait (52, 53). Each RG is thought to contain two excitatory neuron populations representing flexor and extensor half-centers connected by reciprocal inhibition, whose activity defines the flexor and extensor phases of limb movements, respectively. According to the *classical half-center concept* (54), switching between the flexor and extensor activity phases (for review see (55, 56)) occurs through a so-called *release* mechanism (57) based on an adapting (decrementing) activity of each half-center and mutual inhibition between them. This mechanism does not necessarily require the ability of each half-center to intrinsically generate rhythmic activity, and the resultant RG pattern is usually flexor-extensor balanced, so that the durations of both phases are approximately equal.

The other potential mechanism is based on the intrinsic ability of one or both half-centers to generate rhythmic bursting (57-60). Optogenetic studies in the isolated spinal cord have demonstrated that rhythmic flexor and extensor activities can be evoked in certain conditions independent of each other (61), confirming that both flexor and extensor half-centers are *conditional* intrinsic oscillators, i.e. capable of endogenous generation of rhythmic bursting activity. Pearson and Duysens have previously proposed a *flexor-driven* concept (so called *swing*

generator model, (62, 63); for review see (64)), in which only the flexor half-center is intrinsically rhythmic, hence representing a true RG, while the extensor half-center shows sustained activity if uncoupled and exhibits anti-phase oscillations due to rhythmic inhibition from the flexor half-center.

To meet both concepts, we previously suggested that both half-centers are conditional oscillators, whose ability to intrinsically generate rhythmic bursting depends on the level of excitation (12, 53, 65, 66). In this case, a relatively strong excitation of the extensor half-center keeps it in the mode of sustained activity (if uncoupled), whereas a relatively weak excitatory drive to the flexor half-center allows generation of intrinsic oscillations. Therefore, the mechanism for rhythm generation in the RG may vary and, depending on external drives to its half-centers or their level of excitation, it can operate according to the classical half-center or the flexor-driven scenario as was previously demonstrated and analyzed by (67).

In the present study, we extend the RG model of (67) by assuming that increased activation of the flexor half-center is accompanied by a corresponding decrease in the activity of the extensor half-center. To implement this assumption in the model, we suggested that the external excitatory drive to the flexor half-center simultaneously provides inhibition to the extensor half-center, thus reducing the level of its excitation and directing its operation toward intrinsic rhythmicity. To this end, with an increase of the drive to the RG (with the corresponding increase of oscillation frequency) the operating rhythmogenic mechanism changes from the flexor-driven rhythmicity to classical half-center oscillations with a quasi-balanced flexor-extensor pattern.

To study the behaviors of the proposed RGs in the context of left-right interactions and limb coordination, we incorporated these new RG implementations in the model of left-right circuit interactions in the spinal cord previously described by (10). The resultant model included

two (left and right) RGs interacting via several commissural pathways presumably mediated by genetically identified $V0_V$, $V0_D$ and V3 interneurons. The main goal of this study was to investigate left-right interactions and coordination under different symmetric and asymmetric conditions, which were defined by the same or different drives to left and right RGs, respectively. We assumed these conditions to be, at first approximation, similar to overground or regular tied-belt treadmill locomotion in cats (symmetric conditions) and their stepping on split-belt treadmills with different speeds of the left and right belts (asymmetric conditions). The experimental data were collected from intact and spinal cats in previously published (4, 5, 68) and new experiments. These experimental data were compared with the results of our simulations, in which the modelled circuits operated in similar symmetric and asymmetric conditions. We used these comparisons to evaluate the plausibility of our model and, thus, to formulate important insights into the organization of spinal CPG circuits and their role in limb coordination during locomotion.

3.2 Methods

3.2.1 Experimental studies

Ethical approval

All procedures were approved by the Animal Care Committee of the Université de Sherbrooke in accordance with policies and directives of the Canadian Council on Animal Care (Protocol 442-18). The current dataset was obtained from 11 adult cats (7 females and 4 males) weighing between 3.5 and 5.0 kg. However, only 1 new cat contributed new data during overground locomotion, as data from previous studies were reanalyzed (5) or reused (4) for

illustrative or modeling purposes. Before and after experiments, cats were housed and fed in a dedicated room within the animal care facility of the Faculty of Medicine and Health Sciences at the Université de Sherbrooke. As part of our effort to maximize the scientific output of each animal, 10 of 11 animals were used in other studies to answer different scientific questions (4, 5, 68-82). The experimental studies complied with the ARRIVE guidelines (83) and principles of animal research established by the Journal of Physiology (84).

Surgical procedures

Surgical procedures were described in detail in (4, 5) and also apply to the new cat used here. Briefly, we performed all surgical procedures in an operating room with sterilized equipment. Before surgery, the cat was sedated with an intramuscular (i.m) injection of Butorphanol (0.4 mg/kg), Acepromazine (0.1 mg/kg), and Glycopyrrolate (0.01 mg/kg). Induction was done with Ketamine/Diazepam (0.11 ml/kg in a 1:1 ratio, i.m.). The fur overlying the back, stomach, and hindlimbs was shaved. The cat was then anesthetized with isoflurane (1.5 - 3%) using a mask for a minimum of 5 min and then intubated with a flexible endotracheal tube. We confirmed isoflurane concentration during surgery by monitoring cardiac and respiratory rates, by applying pressure to the paw to detect limb withdrawal, and by assessing muscle tone. A rectal thermometer was used to monitor body temperature and keep it between 35°-37°C using a water-filled heating pad placed under the animal and an infrared lamp positioned ~50 cm above the cat. During each surgery, we injected an antibiotic (Convenia, 0.1 ml/kg) subcutaneously and a transdermal fentanyl patch (25 mcg/hr) was taped to the back of the animal 2-3 cm rostral to the base of the tail. During surgery and approximately seven hours later, another analgesic (Buprenorphine 0.01 mg/kg) was administered subcutaneously. After surgery, cats were placed in an incubator and closely

monitored until they regained consciousness. At the conclusion of the experiments, cats received a lethal dose of pentobarbital through the left or right cephalic vein.

Spinal transection. The spinal cord was completely transected at low thoracic levels in six cats (4 females, 2 males); see (4). A small laminectomy was performed between the junction of the 12th and 13th vertebrae. After exposing the spinal cord, lidocaine (Xylocaine, 2%) was applied topically and injected within the spinal cord. The spinal cord was then transected with surgical scissors. Haemostatic material (Spongostan) was then inserted within the gap and muscles and skin were sewn back to close the opening in anatomic layers. Following spinalization and for the remainder of the study, the bladder was manually expressed 1–2 times each day. The hindlimbs were frequently cleaned by placing the lower half of the body in a warm soapy bath. For training the recovery of hindlimb locomotion see (4).

Implantation. All 11 cats were implanted with electrodes to chronically record muscle activity (EMG, electromyography). Pairs of Teflon insulated multistrain fine wires (AS633; Cooner wire, Chatsworth, CA) were directed subcutaneously from 1-2 head-mounted 34-pin connectors (Omnetics Connector Corporation, Minneapolis, MN) and sewn into the belly of selected hindlimb muscles for bipolar recordings. We verified electrode placement by electrically stimulating each muscle through the appropriate head connector channel.

Experimental paradigms: Experiments in the 10 cats from previous studies (Frigon et al. 2015, 2017 (4, 5)) were performed on an animal treadmill with two independently controlled running surfaces 120 cm long and 30 cm wide (Bertec Corporation, Columbus, OH). Cats

performed three locomotor paradigms: 1) Tied-belt locomotion from 0.1 m/s (spinal cats) or 0.4 m/s (intact cats) up to 1.0 m/s in 0.1 m/s increments; 2) split-belt locomotion with one side (slow side) stepping at 0.4 m/s and the other side (fast side) stepping from 0.5 m/s to 1.0 m/s in 0.1 m/s increments; 3) split-belt locomotion with the slow side stepping at 0.1 m/s and the fast side stepping from 0.2 m/s to 1.0 m/s in 0.1 m/s increments (spinal cats only). In spinal cats, the forelimbs remained on a stationary platform with a Plexiglas separator placed between hindlimbs. In the cat that contributed new data, we trained the animal to step along an oval-shaped walkway at self-selected speeds. The walkway has 2.07 m straight paths (0.32 m wide) on each side and we only analyzed data during straight path stepping.

Data acquisition and analysis. Videos of the left and right sides during overground and treadmill locomotion were captured with two cameras (Basler AcA640-100 gm) at 60 frames per second with a spatial resolution of 640 by 480 pixels. A custom-made Labview program acquired images and synchronized the cameras with the EMG. Videos were analyzed off-line at 60 frames per second using custom-made software. Contact of the paw and its most caudal displacement were determined for both hindlimbs by visual inspection. We defined paw contact as the first frame where the paw made visible contact with the treadmill surface while the most caudal displacement of the limb was the frame with the most caudal displacement of the toe. We measured cycle duration from successive contacts of the same hindpaw while stance duration corresponded to the interval of time from paw contact to the most caudal displacement of the limb. Swing duration was measured as cycle duration minus stance duration. Durations from 6-15 cycles for each limb were averaged for an episode during treadmill locomotion. In one cat, we obtained and analyzed 44 cycles from 10 runs of overground locomotion.

The EMG was pre-amplified (x10, custom-made system), bandpass filtered (30–1000 Hz) and amplified (x100–5000) using a 16-channel amplifier (AM Systems Model 3500, Sequim, WA). EMG data were digitized (2000 Hz) with a National Instruments card (NI 6032E) and acquired with custom-made acquisition software and stored on computer. The EMG data set shown came from recordings in the anterior sartorius (Srt, hip flexor/knee extensor), the vastus lateralis (VL, knee extensor) and and the lateral gastrocnemius (LG, ankle plantarflexor/knee flexor).

3.2.2 Mathematical Modeling

We implemented a reduced mathematical model based on the work of (53). Simulating flexor and extensor half-centers using activity-based neuron models describing neuron populations (85) significantly simplifies mathematical analysis. The voltage variable of each flexor and extensor units represents the average voltage of the population of flexor and extensor neurons. Such a reduction provides an accurate description of the network dynamics in the CPG controlling mammalian locomotion (1, 67). The CPG network controlling rhythmic locomotion is known to include both excitatory and inhibitory connections between flexor half-centers (1, 10, 52, 53, 65, 66, 86, 87). We only included reciprocal inhibition between flexors in the model assuming a net inhibitory interaction. Flexor and extensor half-centers comprising left and right RGs also inhibit each other. Additionally, the model included inhibition from extensors to contralateral flexors. This connection was first introduced by (53) who found that inhibition of flexor half-centers by contralateral extensor stabilize anti-phase left-right alternations in corresponding gaits. In this study we show that this interaction is essential for symmetric left-right alternations and explain the mechanism.

All neurons were modeled using the formalism described in (88) and then used in a number of previous publications (1, 10, 53, 65, 67, 87, 89-91). Intrinsic bursting properties resulted from slowly inactivating sodium current dynamics. The membrane potential (*V*) of flexors and extensors was governed by the following equation:

$$C\frac{dV}{dt} = -I_L - I_{NaP} - I_{syn}. \quad (1)$$

Here, C is the capacitance, t is time, I_L is the leak current, I_{NaP} is the slowly inactivating (persistent) sodium current, and I_{syn} is the synaptic current that is the sum of input currents from other neurons and the excitatory drive current. The leak current and the persistent sodium current were defined in the same manner in flexors and in extensors.

$$I_L = g_L(V - E_L); \quad (2)$$

$$I_{NaP} = g_{NaP} m_{NaP\infty}(V) h_{NaP}(V - E_{Na}). \quad (3)$$

In the expression for the leak current (2), g_L is the conductance of the leak current and E_L is the leak reversal potential. In the expression for the persistent sodium current (3), g_{NaP} is the persistent sodium maximal conductance and E_{Na} is the sodium reversal potential. $m_{NaP\infty}(V)$ is the voltage-dependent steady-state activation function of the persistent sodium current. Persistent sodium current activation is considered to be instantaneous. h_{NaP} is the persistent sodium inactivation gating variable. The steady state activation functions for persistent sodium activation and inactivation are given by the following expressions:

$$m_{NaP\infty}(V) = \left(1 + \mathrm{e}^{\frac{V - V_{mNaP}}{k_{mNaP}}}\right)^{-1}; \quad (4)$$

$$h_{NaP\infty}(V) = \left(1 + \mathrm{e}^{\frac{V - V_{hNaP}}{k_{hNaP}}}\right)^{-1}, \quad (5)$$

and the dynamics of the persistent sodium inactivation variable were governed by the following differential equation:

$$\tau_{NaP}(V)\frac{dh_{NaP}}{dt} = h_{NaP\infty}(V) - h_{NaP}; \quad (6)$$

$$\tau_{NaP}(V) = \tau_{NaP}/\cosh\left(\frac{V - V_{\tau NaP}}{k_{\tau NaP}}\right). \quad (7)$$

Here, $\tau_{NaP}(V)$ is the voltage-dependent time constant for the inactivation of the persistent sodium current. In the gating variable expressions, V_{xNaP} is the half-(in) activation voltage and k_{xNaP} is the (in)activation slope, where $x \in \{m, h, \tau\}$.

In the differential equation for the membrane potential the third current is the synaptic current I_{syn} and is defined by the synaptic input from neurons in the network as well as external drives. For flexors, this included input from the contralateral flexor, the ipsilateral extensor, and the contralateral extensor. For extensors, the synaptic current included input from the ipsilateral flexor. In flexors and extensors, drive was implemented as the conductance of an excitatory input. The general expression for the synaptic current in neuron i is as follows:

$$I_{syni} = d_i(V - E_{ex}) + \sum_{j=1}^{4} b_{ji} f(V_j)(V_i - E_{inh}). \quad (8)$$

Here, d_i is the excitatory drive to neuron i and V_i is the voltage of neuron i. E_{ex} is the reversal potential for the excitatory synaptic currents. I_{syni} includes the sum over all synaptic inputs from $j = 1{:}4$ (see Fig. 2.1). E_{inh} is the reversal potential for the inhibitory synaptic currents. b_{ji} is the weight of the synaptic connection from neuron j to neuron i, which represents the maximal conductance of the corresponding synaptic channel. $f(V)$ is the activity (normalized firing rate) as a function of voltage and is defined by the following piecewise linear function.

$$f(V) = \begin{cases} 0, V < V_{min}; \\ \frac{V - V_{min}}{V_{max} - V_{min}}, V_{min} \le V \le V_{max}; \\ 1, V > V_{max}. \end{cases} \quad (9)$$

The activity function $f(V)$ varies from 0 to 1. Here, V_{min} and V_{max} define the voltages at which threshold and saturation are reached, respectively. The values of all parameters are provided in Table 1. In our simulations, the synaptic weights of commissural connections b_{12}, b_{21}, b_{41} and b_{32} were varied, while synaptic weights within each RG b_{31}, b_{42}, b_{13} and b_{24} were fixed.

Membrane capacitance (pF)	$C = 20$
Maximal conductance (nS)	$\bar{g}_L = 2.8$, $\bar{g}_{NaP} = 5$
Reversal potentials (mV)	$E_L = -65$, $E_{NaP} = 50$, $E_e = -10$, $E_i = -90$
Synaptic weights	$b_{12} = b_{21}$, $b_{41} = b_{32}$, $b_{31} = b_{42} = 0.5$, $b_{13} = b_{24} = 1$
$f(V)$ parameters (mV)	$V_{\min} = -50$, $V_{\max} = 0$
Time constant (ms)	$\tau_{NaP} = 1500$
I_{NaP} parameters (mV)	$V_{mNaP} = -40$, $k_{mNaP} = -6$, $V_{hNaP} = -50$, $k_{hNaP} = 10$, $V_{\tau NaP} = -100$, $k_{\tau NaP} = 40$

Table 3.1 Model Parameter Values

3.3 Results ~ Modeling Spinal CPG Circuits

3.3.1 Model of rhythm generator (RG) controlling single limb

In the present study, we accepted the model of (67) and their suggestion that rhythmic activity in the RG may be based on flexor-driven or classical half-center mechanisms, depending on the level of excitation of flexor and extensor half-centers, both considered conditional bursters. They independently varied flexor and extensor drives and identified parameter areas in which the above mechanisms operate. Here, we extended the model of Ausborn et al. by using the assumption that an increase in activation of the flexor half-center is accompanied by a decrease in the activity of the extensor half-center. Specifically, we assumed that the excitatory drive to the flexor half-center provides inhibition to the extensor half-center (through inhibitory interneurons), reducing the initial level of its excitation (Fig. 3.1 A, B). In this case, at relatively low drives to the flexor half-center, the frequency of RG oscillations (defined by flexor activity) is low, and the

locomotor pattern is not balanced, i.e., has a short flexor and long extensor bursts. An increase in the drive to the flexor half-center increases the RG frequency, making the pattern more flexor-extensor balanced while concurrently reducing the level of excitation of the extensor half-center, shifting the extensor half-center's operation towards an intrinsically rhythmic state. Figure 3.1C shows a two-parameter frequency dependence on flexor and extensor drives similar to shown in (67) that was calculated for a set of parameters used in the present study. According to our suggestion, with the changes in the drive to flexor half-center (Drive to F) and the net drive to extensor half-center (Drive to E minus Drive to F), the parameter point representing a state of RG operation moves along the yellow line intersecting both areas for flexor-driven and classical half-center oscillations (Fig. 3.1C). Specifically, with an increase of drive to flexor center, the RG operation regimes shifts from the flexor-driven intrinsic oscillations (with short flexor bursts and long extensor bursts, Fig. 3.1D1) toward the classical half-center mechanism of rhythmicity with a quasi-balanced flexor-extensor pattern (Fig. 3.1D2).

Figure 3.1 **Proposed organization of the single rhythm generator (RG)**.

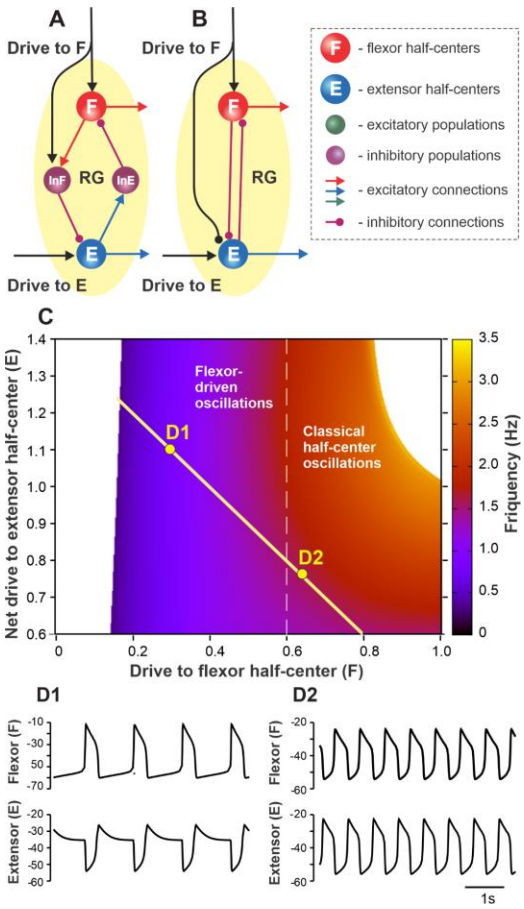

A. Each RG consists of flexor (F) and extensor (E) neural populations (half-centers) inhibiting each other via inhibitory interneuron populations InE and InF. Flexor and Extensor half-centers receive excitatory drives labelled as Drive to F and Drive to E, respectively. Drive to F also excites InF and thus has an inhibitory effect on the extensor half-center. **B**. The simplified model schematic. The inhibitory interneuron pathways are replaced with direct reciprocal inhibition between flexor and extensor half-centers. The net drive to the extensor half-center is defined by the excitatory Drive to E and inhibition from Drive to F. **C**. The dependence of RG bursting frequency on the drive to the flexor half-center and the net drive to the extensor half-center. A flexor-driven rhythm occurs in the region with relatively high drive to the extensor and low drive to the flexor, i.e. where the flexor half-center is intrinsically rhythmic (to the left from the vertical dashed line). Classical half-center oscillations occur to the right from the vertical dashed line where both flexor and extensor half-centers exhibit tonic activity if decoupled. The hypothetical dependence of the net extensor drive on the flexor drive is shown by yellow line – as the flexor drive increases the net extensor drive decreases due to inhibition from Drive to F to the extensor half-center (see panels A, B). **D1-D2**. Simulated flexor (above) and extensor (below) activity traces for the parameter points labelled as D1 and D2 in panel C.

In Fig. 3.1 the representation of panel **C** follows (67) methods.

3.3.2 Commissural interactions between RGs controlling left and right limbs

The main goal of this study was to investigate left-right coordination of limb movements under different symmetric and asymmetric conditions. Left-right limb coordination supposedly relies on neural interactions between the two RGs controlling the left and right limbs. The connectome of these interactions was drawn from the model of (10). In that model, the left and right RGs interacted via three commissural pathways (Fig. 3.2A). Two of them, mediated by genetically identified inhibitory $V0_D$ and excitatory V0v (V2a-V0v paths, acting via the inhibitory Ini populations) populations of commissural interneurons (CINs), promoted left-right alternation (92) through mutual inhibition between the left and right flexor half-centers (see also (1, 12)). The third pathway, mediated by genetically identified V3 CINs, promoted left-right synchronization via mutual excitation between the left and right extensor half-centers and diagonal inhibition of the contralateral flexor half-centers (10); see Fig. 3.2A. In the present study, to simplify the model and make it more mathematically tractable, all commissural interactions were replaced by functionally equivalent direct connections, as shown in Fig. 3.2B.

Figure 3.2 **Network interactions between left and right RGs**.

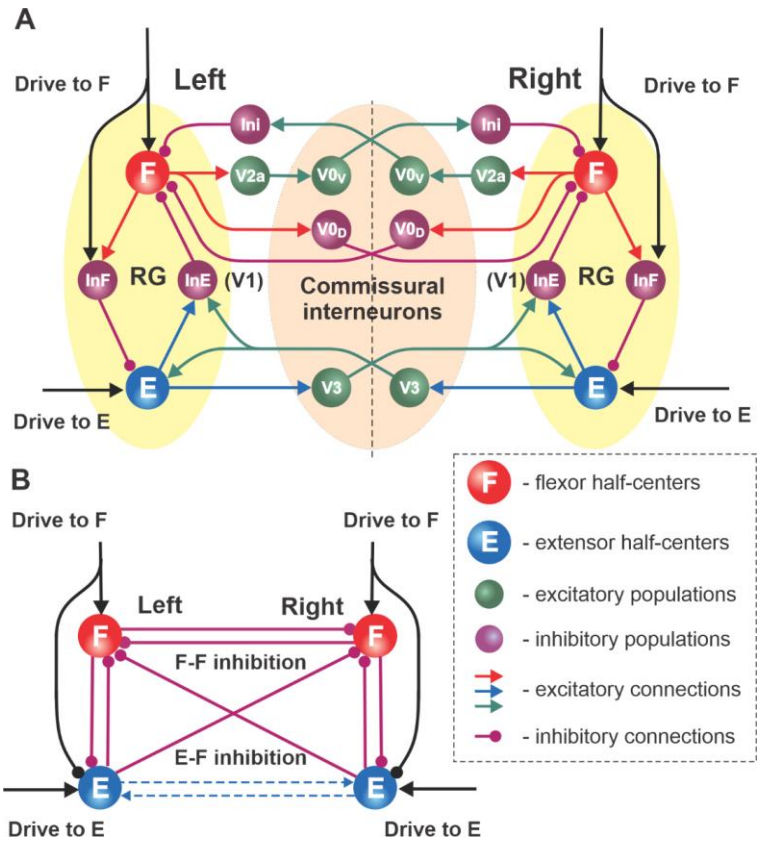

A. Commissural Interactions between left and right locomotor rhythm generators (RGs) proposed by Danner *et al.* 2019. The left and right RGs interact through several commissural pathways mediated by different commissural interneurons (CINs): $V0_V$, $V0_D$, and V3 types. **B.** Schematic of the reduced model; all CIN-mediated connections are replaced with direct synaptic interactions. The net interactions are inhibitory (excitatory interactions are excluded - dashed lines). It is suggested that external drives excite flexor (F) and inhibit extensor (E) centers.

In Fig. 3.2 panel **A** is modified from (10) Fig. 5 in with permission.

3.3.3 Speed-dependent changes in phase durations during left-right symmetric and asymmetric locomotion

Our objectives was to evaluate the RG circuit organization proposed above by considering their operation in two cases: a symmetric case, when left and right drives vary but remain equal, and an asymmetric case, when one of two drives changes while the other maintains a constant value. We assumed that these two regimes are functionally comparable to regular overground or tied-belt treadmill locomotion (symmetric case) and split-belt treadmill locomotion with different speeds for the left and right belts (asymmetric case). We focused on the analysis of speed-dependent changes in the durations of the main locomotor phases (swing and stance) using data from previous experiments during tied-belt and split-belt treadmill locomotion in intact and spinal cats (4, 5) and new experiments performed during overground locomotion in an intact cat.

3.4 Results ~ Speed-dependent changes in phase durations during left-right symmetric locomotion

3.4.1 Left-right symmetric locomotion in cats

Figure 3.3 shows changes in the cycle duration and durations of swing and stance phases (panel A) and raw activity of representative flexor (Srt) and extensor (LG) muscles (panels B1-B3) during overground locomotion at different self-selected speeds in a freely stepping intact cat. Panels C and D show cycle and phase durations in a group of intact and spinal cats, respectively, during tied-belt treadmill locomotion. In all of these cases, an increase in speed was accompanied by a substantial reduction of stance phase duration with small or absent changes in swing phase

duration, consistent with previous studies in cats (4, 69, 70, 93, 94). An interesting difference between the three cases shown in Fig. 3.3 is that during overground locomotion in intact cats, at a speed of ~1.1 m/s, the swing and stance phase durations become equal and then at higher speeds, stance becomes shorter than swing (Fig. 3.3A). Despite a similar tendency, stance did not become shorter than swing during tied-belt treadmill locomotion in intact (Fig. 3.3C) or spinal (Fig. 3.3D) cats. The treadmill locomotion is not usually performed at speeds greater than 1.0 m/s in intact cats, because of safety concerns, as well as in spinal cats, in which the pattern starts to break down. Nevertheless, spinal cats reached swing-stance equality at about 1.0 m/s (Fig. 3.3D).

Figure 3.3 **Locomotor cycle and phase durations and muscle activity during overground and tied-belt locomotion across intact and spinal cats.**

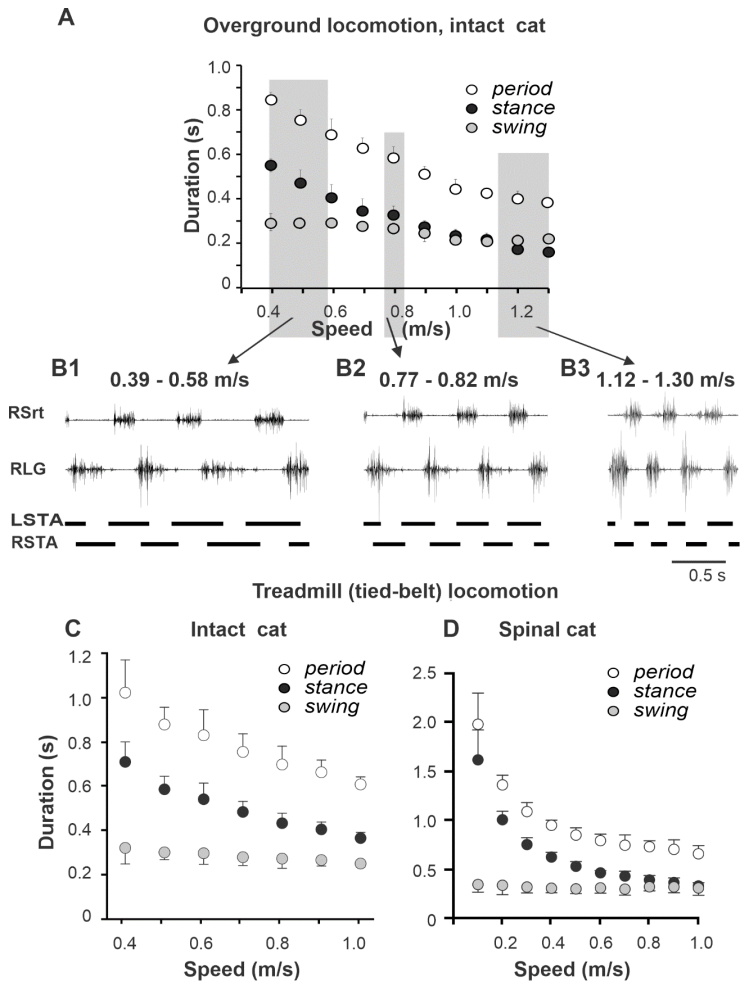

A. Cycle and phase durations for the right hindlimb during overground locomotion in an intact cat. The cat stepped in an oval-shaped walkway with 2.07 m straight paths and spontaneously changed speed. We analyzed data from 46 cycles obtained in one session and averaged into 10 bins by rounding to the nearest body speed in 0.1 m/s increments (each data point is the mean ± standard deviation). Note the absence of standard deviations when we only obtained 1 cycle at some speeds. **B1-B3**. Hindlimb muscle activity and phase durations during overground locomotion at 0.39-0.58 m/s, 0.77-0.82 m/s, and 1.12-1.30 m/s in one intact cat. The black horizontal bars at the bottom of each panel show left (LSTA) and right (RSTA) stance phase durations. RLG, right lateral gastrocnemius; RSrt, right sartorius. **C-D.** Cycle and phase durations for the right hindlimb during tied-belt treadmill locomotion in (**C**) intact and (**D**) spinal cats across speeds. We obtained 6-15 cycles in 7 intact and 6 spinal cats and averaged cycle and phase durations for each cat. Each data point is the mean ± standard deviation for the group of intact and spinal cats.

In Fig. 3.3 panels **C** and **D** are, respectively, modified from Fig. 2B in (5) and reproduced from Fig. 2A in (4), with permission.

3.4.2 Simulation of left-right symmetric regime with the model

The schematic of our simplified model is shown in Fig. 3.2B. In this model there are mutual inhibitory interactions between the flexor half-centers, which combine and simplify two inhibitory pathways mediated by $V0_D$ and $V0_V$ CINs in Fig. 3.2A. This inhibition is referred as "flexor-flexor" (or F-F) inhibition. In addition, there are also inhibitory pathways from each extensor half-center to the contralateral flexor half-center (Fig. 3.2A), which are presumably mediated by V3 CINs through inhibitory populations, such as V1 (10). The strength of this connection in the present model is referred to as "extensor-flexor" (or E-F) inhibition. We therefore have four control parameters in the model: the drives to both flexor half-centers (which also define the inhibitory inputs to the extensor half-centers; these drives are equal in the symmetrical case) and F-F and E-F inhibitions.

First, we simulated the changes in locomotor phase durations in response to increasing drive to a single RG (Fig. 3.4). The external drive to the RGs was increased from 0.2 to 0.8 producing progressively shorter extension at relatively constant flexion duration. With an increase of external drive, the frequency of oscillations increased from about 0.4 to about 1.4 Hz. The increase in frequency (decrease in the period of oscillations) occurred mainly by shortening the extensor phase with minor changes in the duration of the flexor phase. The predominant decrease in extensor phase qualitatively corresponds to the change in the duration of stance and swing phases observed with increasing locomotor speed in experimental studies (Fig 3.3A). Note that in our simulations, the flexor and extensor phases become equal at drive values of about 0.7, after which extension becomes shorter than flexion (similar to that in Fig. 3.3A). This reversal in flexor-extensor durations occurs in our model because flexor and extensor half-centers receive the same external excitation at a drive value of approximately 0.7 (see Fig. 3.1C).

Figure 3.4 **Dependence of the period, flexion and extension on drive to flexor in the model of single RG.**

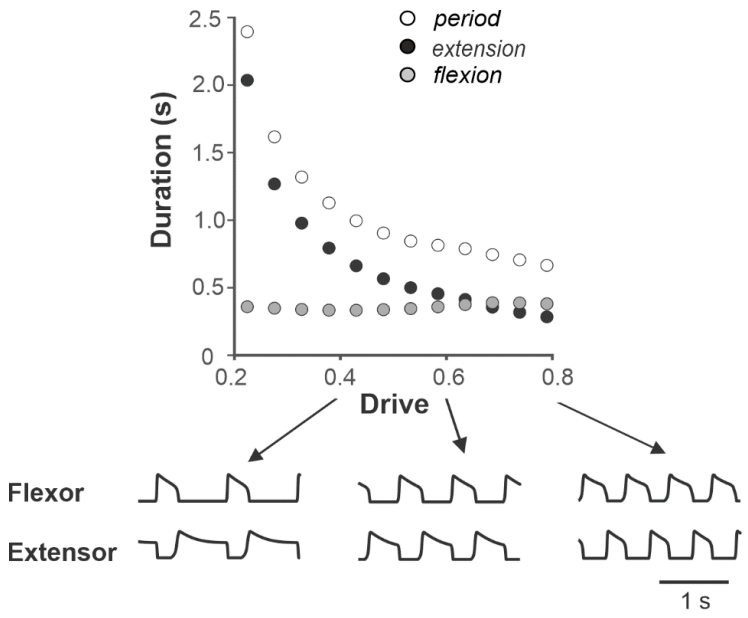

Simulations show decreasing duration of extension and relatively constant flexion with increasing drive similar to that during overground tied-belt locomotion in cats with increasing locomotor speed (Fig. 3.3). Below, exemplar activity traces of flexor and extensor half-centers are shown for low (0.4), medium (0.6) and high (0.8) drive to flexor values.

To explore the system's behavior in terms of left-right coordination, we simulated the model and identified synchronization patterns while varying inhibition strengths at different drive values. Figure 3.5A-D shows the parameter plane partitions for four representative drive values corresponding to low and high frequencies. Qualitatively, the F-F inhibition promotes alternating (anti-phase) flexor activity while the E-F inhibition contributes to synchronizing (in-phase) the flexor half-centers due to a phasic reduction in inhibition of flexors during contralateral flexion. Therefore, it is reasonable to expect that at high F-F inhibition and low E-F inhibition (an upper-left corner on Fig. 3.5 diagrams), the left and right RGs exhibit alternating activity, and at low F-

F inhibition and high E-F inhibition their activity synchronizes at all frequencies. These regimes of exact anti-phase and in-phase oscillations are observed in the white and black parameter regions, respectively. There is an overlap between the two regions (shown in grey), which corresponds to bistability in the system, where both regimes can operate depending on the initial conditions chosen. A transition from in-phase to anti-phase oscillations occurs at the boundary between the grey and white regions, which is invariant to the drive (Fig. 3.5A-D). An opposite transition occurs at the grey-black boundary, which moves up in terms of F-F inhibition with the drive, thus reducing the bistability area.

There are also regimes of asymmetric alternations at relatively low (Fig. 3.5A, orange region) and high (Fig. 3.5C, D yellow region) drive values corresponding to low or high locomotor frequencies. At low frequencies (i.e. low drive values), this regime is observed at low values of E-F inhibition; it results from post-inhibitory rebound activation of the flexor oscillator after the contralateral flexor deactivates. Slightly higher E-F inhibition strength prevents this post-inhibitory rebound by suppressing the contralateral flexor half-centers for the duration of strong extensor activity in the beginning of the extensor burst. At high locomotor frequencies, the asymmetric alternation regime is practically indistinguishable from pure anti-phase oscillations because the duty cycle is very close to 1/2.

Based on the analysis above, we found that the considered circuit produces robust anti-phase alternations of flexor activity in a certain parameter region for all locomotor frequencies. We chose the exemplary point (0.2, 0.4) that belongs to this region for subsequent simulations. However, this particular choice did not make a qualitative difference in the system's behavior as long as the parameter point chosen belonged to the region of monostable anti-phase oscillations.

Figure 3.5 **Partitioning of the parameter plane for different coordination patterns**.

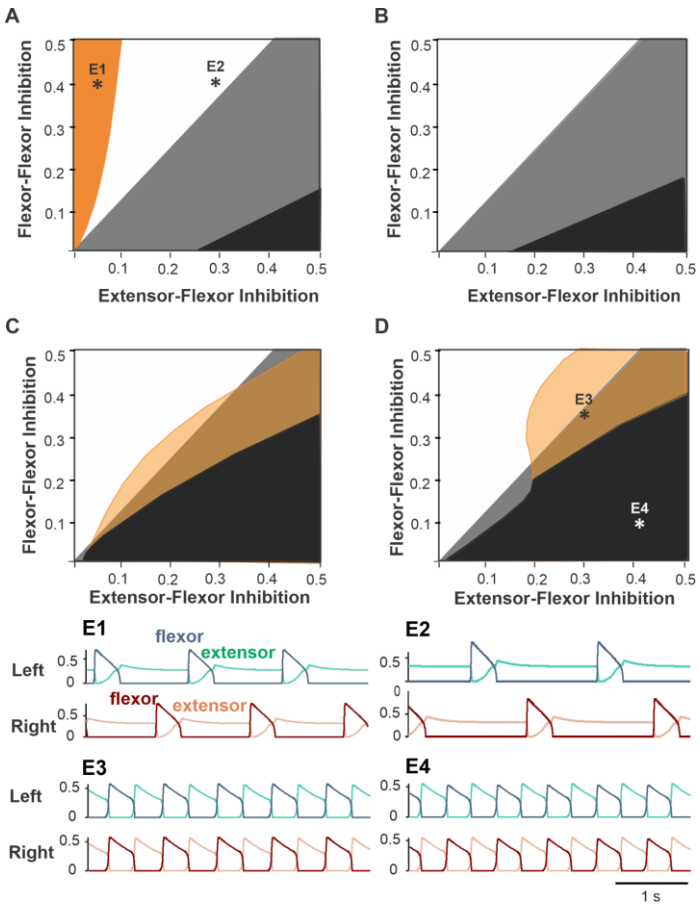

The areas of regimes with different phase relationship between activities of left and right flexor half-centers are shown for varying flexor-flexor (F-F) inhibition and varying crossing extensor-flexor (E-F) inhibition at four different flexor drive values equal to left and right sides (symmetric case). **A**. Drive = 0.3. Orange region: asymmetric alternations of left and right flexor activity – see example activity traces in panel **E1**. The white region corresponds to exact anti-phase left-right alternations (see panel **E2** for an example. The black region corresponds to in-phase left-right synchronization like in panel **E4**. Bistability occurs in the gray region as antiphase and in-phase regimes coexist and can be realized depending on initial conditions. **B**. Drive = 0.4. As we increase drive, the orange region disappears, and the black region of in-phase synchronization grows in size. **C**. Drive = 0.5. With relatively high drive to flexors a new region appears (shown by transparent orange) with small phase difference between flexors (see panel **E3** for an example). The black region of in-phase synchronization increases further. **D**. Drive = 0.65. **E1-E4.** Activity traces of left flexors (blue) and extensors (green) above and the right flexors (dark brown) and extensors (light brown) below corresponding to parameter points labeled accordingly in panels A and D. **E1**. Drive = 0.3, F-F inhibition = 0.4, E-F inhibition = 0.05. **E2.** Drive = 0.3, F-F inhibition = 0.4, E-F inhibition = 0.3. **E3.** Drive = 0.65, F-F inhibition = 0.1, E-F inhibition = 0.4. **E4**. Drive = 0.65, F-F inhibition = 0.33, E-F inhibition = 0.3.

3.5 Results ~ Speed-dependent changes in phase durations and synchronization patterns during left-right asymmetric locomotion

3.5.1 Left-right asymmetric locomotion in cats walking on split-belt treadmills

The split-belt treadmill locomotion experiments, in which animals step on belts with different speeds for the left and right sides, is a common way to study limb coordination during locomotion in cats and humans. Many previous studies in cats demonstrated that both intact and spinal animals adapt to such stepping conditions and demonstrate stable locomotion (4, 5, 9, 68, 69, 72, 95). In these studies, we can separate cat locomotion on the split-belt treadmill in two qualitatively different types of conditions: *simple* and *extreme* (4, 68). In the simple condition, characterized by a relatively small speed difference between moving belts, animals maintain a 1:1 ratio between the number of steps made by left and right limbs. In *extreme* conditions, the animal starts taking more steps on the fast side compared to the slow side resulting in step ratios of 1:2, 1:3, 1:4, etc. (4, 5, 9).

The changes in locomotor phase durations during split-belt locomotion of intact and spinal cats in *simple* conditions are shown in Fig. 3.6; see also (4, 5). In both cases, the slow hindlimb (SHL) stepped at a constant speed of 0.4 m/s, whereas the speed of the fast hindlimb (FHL) belt increased from 0.5 to 1.0 m/s. In these conditions, the important characteristics of locomotion observed are (see also (4, 5)): (1) The step cycle period remains equal in both hindlimbs (FHL and SHL). (2) In the SHL, the durations of swing and stance phases do not change much. (3) In the FHL, the duration of stance decreases, whereas the duration of swing increases allowing step cycle duration to remain relatively unchanged despite an increase in speed of the FHL. At a FHL speed

of ~0.8 m/s, the durations of swing and stance phases become approximately equal and then the swing phase becomes longer than the stance phase at faster FHL speeds (Fig. 3.6B, right).

The locomotor characteristics of intact and spinal cats differ in *extreme* conditions, when the speed ratio between the slow and fast belts are set to 1:3 and more, up to 1:10 (4, 68). In this case, the locomotor pattern changes in such a way that cats take more steps on the fast side than on the slow side. Specifically, at 1:3 and 1:4 speed ratios, the limbs on the fast side perform 2-3 steps for every step of the limb on the slow side (1:2 and 1:3 coordination pattern), whereas at ratios of 1:5 or higher, 1:4 and 1:5 coordination pattern were observed (4, 68). Despite inter-animal variability, both intact (68) and spinal (4) cats exhibit 1:2+ coordination patterns.

Figure 3.6 **Cycle and phase durations and muscle activity during split-belt locomotion across intact and spinal cats.**

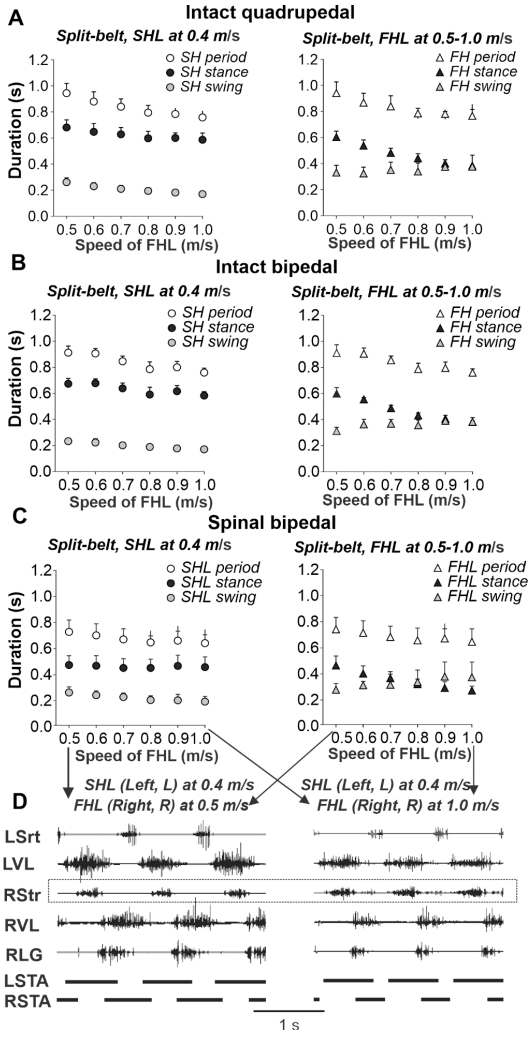

Cycle and phase durations in (**A-B**) intact and (**C**) spinal cats when the slow hindlimb (SHL) was stepping at 0.4 m/s while the fast hindlimb (FHL) stepped from 0.5 to 1.0 m/s in 0.1 m/s increments. Cycle and phase durations are shown for SHL (left panel) and FHL (right panel). We obtained 6-15 cycles in 5 intact and 6 spinal cats and averaged cycle and phase durations for each cat. Each data point is the mean ± standard deviation for the group of intact and spinal cats. **D**. Hindlimb muscle activity and phase durations during split-belt locomotion with the slow limb stepping at 0.4 m/s and the right hindlimb stepping at 0.5 m/s (left panel) and 1.0 m/s (right panel) in one spinal cat. The black horizontal bars at the bottom of each panel show left (LSTA) and right (RSTA) stance phase durations. L, left; R, right; LG, lateral gastrocnemius; Srt, sartorius; VL, vastus lateralis.

In Fig. 3.6 panels **A** and **B** are recalculated based on data shown in Figs. 2D, F in (5), **C** is reproduced from Figs. 5A, B in (4), and **D** is reproduced from Figs. 4A, B in (4) with permission. Data from panel **D** are from cat BL (4).

3.5.2 Modeling asymmetric CPG operation

To simulate asymmetric conditions corresponding to different speeds of the treadmill belts, we varied drives to the left and right RGs in our model independently (Fig. 3.2B), so that if disconnected they would produce unsynchronized flexor/extensor alternations with different frequencies. Due to commissural interactions, the model generated different synchronization patterns depending on parameters. We assumed that the left RG receives a smaller drive. This corresponds to a triangular region above the bisector in the bifurcation diagram shown in Fig. 3.7A. The bisector of the bifurcation diagram corresponds to equal drives, where exact anti-phase left-right alternations of flexor activity are produced at the commissural connection weights chosen.

As we start changing the drives to the fast RG, both RGs remain synchronized (1:1 region in Fig. 3.7A), however left and right oscillations become asymmetric. Flexor bursts in the fast RG occur at progressively shorter intervals after flexor bursts. When the drive to the fast RG becomes significantly larger that the drive to the slow RG, the flexor bursts of the fast RG start occurring immediately when flexor bursts of the slow RG end (Fig. 3.7C). In addition, the duration of the flexor bursts of the fast RG becomes progressively longer (see below in relation to Fig. 3.8A, B). These behaviors correspond to the *simple* asymmetric conditions, described above, where a 1:1 coordination pattern is maintained.

When the frequency of the slow RG is relatively low because of a low drive to the slow RG (left part of the bifurcation diagram in Fig. 3.7A), a transition to *extreme* conditions (1:2+ coordination patterns) occurs as we increase the drive to the fast RG further (see above). In the 1:2 regime, one flexor burst of the slow RG corresponds to two flexor bursts of the fast RG (1:2 area in Fig. 3.7A). In this regime, the first flexor burst of the fast RG starts immediately after the flexor

burst of the slow RG ends (Fig. 3.7D). Further increases in the drive to the left (fast) RG leads to the emergence of 1:3+ patterns (Fig. 3.7E), similar to that observed in *extreme* conditions in intact and spinal cats (see above). Between 1:1 and 1:2 regions, there is an area of intermittent regimes where either one or two flexor bursts can be produced by the fast RG during the extension phase of the slow RG, which is commonly observed experimentally (4).

Figure 3.7 **Coordination patterns in the model with asymmetric drives to left and right RGs**.

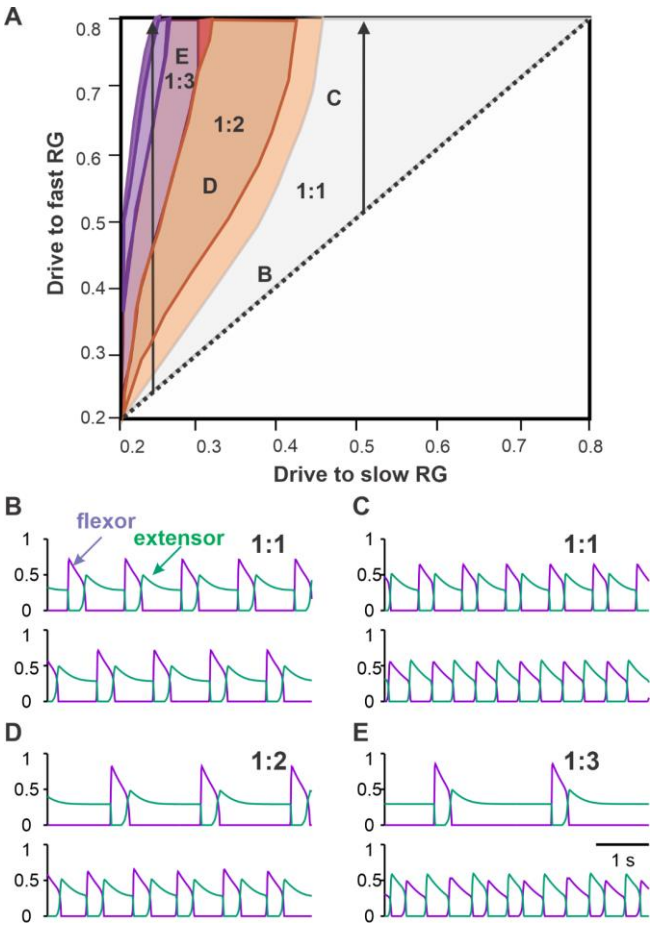

A. Parameter regions corresponding to different numbers of steps on the fast (right) side per one step on the slow (left) side. The region of a single fast flexor burst for each slow flexor burst is labeled 1:1. Regions of multiple right flexor bursts for each left flexor burst are labeled 1:2, 1:3, etc. The left arrow shows regions of 1:2, 1:3 and higher asymmetric gaits with increasing fast flexor drive at a low strength slow flexor drive, corresponding to extreme experimental conditions. The right arrow shows increasing fast flexor drive and a constant slow flexor drive of moderate strength, corresponding to the simple conditions in split-belt experiments. **B-E**. Examples of activity traces are shown for left (above) and right (below) flexors (violet) and extensors (green) corresponding to the parameter points labelled accordingly in panel A. **B**. As in the tied-belt paradigm, symmetric drive distribution to the left and right flexors produces synchronous antiphase oscillations. **C**. As we increase the drive to the right flexor while keeping the drive to the left flexor at 0.5, the gait becomes asymmetric with longer flexion and shorter extension on the fast right side. **D**. When the drive ratio to right and left flexors is high enough, the right flexors bursts twice for every extensor burst in a 1:2 asymmetric gait. **E**. Even higher drive ratio results in three right flexor bursts for each left flexor burst in a 1:3 asymmetric gait.

3.5.3 Changes in locomotor phase duration in a simple asymmetric regime (1:1)

Modeling and analysis of locomotor characteristic changes in the simple condition is more functionally relevant than the *extreme* cases because it occurs frequently during everyday locomotion, such as stepping along a circular path or when turning. Also, these changes provide an indirect test for the CPG organization predicted by the model.

Figure 3.8A, B shows our simulation of such a *simple* asymmetric case, when the drive to the slow RG was kept constant at 0.5, while the drive to the fast RG increased from 0.5 to 0.8 (see the corresponding arrow in Fig. 3.7A). Similar to the experimental studies during split-belt locomotion in a simple asymmetric case shown in Fig. 3.6, despite the left-right asymmetry, the oscillation period remained almost constant and was largely defined by the slow side. Similarly, the durations of flexor and extensor phases were relatively constant on the slow side but changed dramatically on the fast side with increased drive (Fig. 3.8A, B). The most important feature of the simulated behavior (which corresponded to experimental data in Fig. 3.6) was the increased duration of flexion in the fast RG occurring with increased drive to that RG. We can qualitatively explain this phenomenon in the model as follows. On the slow side, the flexor half-center of the slow RG operates in a rhythmic mode, while its extensor half-center operates in a regime of tonic activity (if disconnected) as it receives higher excitatory drive. Therefore, the generation of flexor bursts in the slow RG occurs endogenously after a well-defined recovery period, which is almost unaffected by the synaptic inputs it receives from the other side (fast RG). On the fast side, however, once the net drive to the extensor half center is low enough (recall that based on our assumption an increase in drive to the flexor half-center is accompanied by a decrease in drive to the extensor half-center; see above), the extensor half-center goes into an intrinsically rhythmic mode, meaning that the duration of extension and its interburst intervals start to depend on intrinsic

burst recovery mechanisms. At the same time, the flexor half-center of the fast RG receives increasingly more excitation, so flexor burst termination becomes more dependent on the onset of extensor half-center inhibition rather than on the flexor's endogenous deactivation. With a progressive reduction of net drive to the extensor half-center, the recovery period for extensor activity gets longer, which extends flexion duration. Therefore, the phenomenon of increasing duration of flexion in the fast RG results from changing the rhythmogenesis mechanism in the fast RG from an intrinsic generation of flexor oscillations to the classical half-center mechanism that was implemented in our RG model.

To illustrate this further, we removed inhibitory external inputs to both (left and right) extensor half-centers (that provided the above transition in the rhythmogenic properties of the extensor half-centers) and replaced them with a constant excitatory drive of 0.7 (see Fig. 3.1C). In this case, rhythmogenesis was always based on intrinsic bursting of flexor half-centers without switching to the classical half-center mechanism. The results of these simulations are shown in Fig. 3.8C, D. Note that (a) the duration of the flexor phase on the fast side never increases, and (b) the step-cycle duration on both sides clearly decreases with increasing drive to the fast RG, both contradicting to experimental observations (see Fig. 3.6).

Figure 3.8 **Simulations of asymmetric CPG activity as the drive to the slow (left) flexor is kept constant and the drive to the fast (right) flexor is increasing.**

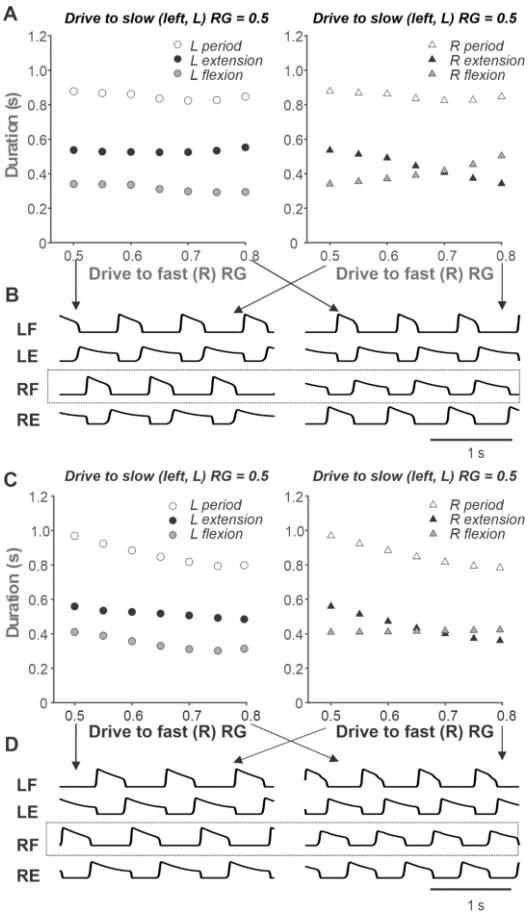

A. The period, flexion and extension duration of the left (slow) and right (fast) RGs as simulated using the model are shown in the left and right panels, respectively. Flexion and extension duration of the slow RG remain fairly constant (left panel). Flexion phase of the fast RG increases in duration while the extension phase of the fast RG shortens in duration (right panel) as in split-belt experiments (see Fig. 3.6). **B**. Activity traces of flexor and extensor half-centers in symmetric conditions (Drive to both flexors = 0.5, left panel) and asymmetric conditions (Drive to slow flexor = 0.5, Drive to fast flexor = 0.8, right panel). **C-D**. For comparison, same as A-B but with inhibitory effect of the flexor drive on the extensor activity excluded from the model. Drive to both extensor half-centers is kept constant at 0.7. **C.** The period, flexion and extension durations of the slow (left) RG all decrease with increasing drive to the fast (right) RG (left panel). The flexion duration of the fast (right) RG remains constant unlike in split-belt experiments. **D**. Flexor and extensor activity traces of left and right RGs for the minimal (0.5) and maximal (0.8) values of the drive to the fast (right) flexor corresponding to simulations in panel C are shown in left and right panels, respectively. L, left; R, right; RG, rhythm generator; LF, left flexor; RF, right flexor; LE, left extensor; RE, right extensor.

3.6 Discussion

3.6.1 Organization and operation of spinal rhythm generators (RGs) controlling limb movements during locomotion

There are currently two major competing concepts concerning the organization and operation of spinal neuronal RGs. In the classical half-center concept (54), flexor and extensor half-centers do not require intrinsic rhythmic properties (for review see (55, 56)). Both half-centers operate in qualitatively similar conditions with phase switching defined by a release mechanism (57) that is based on adapting (decrementing) activity of each half-center and mutual inhibition between them. In the classical half-center, the durations of flexor and extensor phases are balanced (or equal). These durations and the corresponding duty cycles can be easily changed by the level of half-center activation or by external drive. At the same time, the control of RG oscillation frequency in this case is problematic as the oscillation period is not very sensitive to the external drive in half-center oscillators (96).

In contrast, with the flexor-driven concept (62, 63), the RG rhythm and pattern is defined by the intrinsically rhythmic flexor half-center, while the extensor half-center has sustained activity if uncoupled and only exhibits rhythmic bursting through rhythmic inhibition from the flexor half-center (for review see (64)). Thus, the frequency of intrinsically generated flexor bursting explicitly depends on flexor half-center excitation. The distinctive feature of this regime is that the flexor bust duration does not change much and most previously suggested intrinsic oscillatory mechanisms, such as those based on intracellular dynamics of ionic concentrations or slow inactivation of ionic channels (1, 97), produce duty cycles of bursting usually less than 0.5 and are likely to operate at low frequencies with short flexor phases and long extensor bursts.

Both concepts have support in certain conditions. (67) demonstrated that both mechanisms can operate depending on the state of half-centers defined by their level of excitation. Here, we used and refined this idea, by suggesting that (a) at low frequencies the extensor half-center is highly excited and operates in a regime of tonic activity, and (b) an increase in excitation of the flexor half-center, which initially operates in the intrinsic bursting regime, is accompanied by a decrease of excitation of the extensor half-center. Mechanistically, such a decrease of the extensor half-center activation may result from a reduction of excitatory afferent inputs to the extensor half-center when unloading the limb at the stance-to-swing transition (98, 99). With concurrent increases in flexor and extensor drives, the RG transitions from a flexor-driven mechanism (when the frequency changes mostly with extension duration while flexion duration remains relatively unchanged) to the classical half-center mechanism (when stepping is controlled by changes in the duty cycle at a relatively constant frequency).

To test this idea, we incorporated the above RGs in a model of spinal CPG circuits with reciprocal commissural interactions and used this bilateral RG model to simulate speed-dependent changes in the locomotor pattern of intact and spinal cats in symmetrical (during overground and tied-belt locomotion) and asymmetrical (during split-belt treadmill locomotion) conditions. The experimental data from previously published (4, 5, 68) and new experiments were analyzed. The model reproduced and explained a series of experimental findings, including (a) the reversal in flexor and extensor phase durations with an increase of locomotor speed during left-right symmetric locomotion, and (b) the maintenance of step cycle period during split-belt locomotion due to adjustment of the flexor duty cycle. The results of these simulations provide strong support for the proposed organization and operation of spinal locomotor circuits.

3.6.2 Organization of left-right commissural interactions in the spinal cord: the role of V3-mediated commissural pathways

In the present model, the interactions between left and right RGs were based on the model by (10). Importantly, that model was derived from experiments on symmetric (bilateral) and asymmetric (unilateral) optogenetic stimulations of commissural V3 neurons involved in left-right coordination performed in the same study. Interestingly, unilateral stimulation produced effects that were qualitatively similar to some features of split-belt locomotion. They provided strong evidence that spinal V3 CINs are involved in left-right limb coordination via two pathways: through mutual excitation between the left and right extensor half centers of the RGs and, importantly, via crossed inhibition from extensor half-centers to contralateral flexor half centers through an additional inhibitory interneuron population (presumably V1) (see. Fig. 3.2A). In the present study, we show that the commissural inhibition of flexor half-centers by the contralateral extensor half-centers (see Fig. 3.5 and related texts) is critically important for the stability of anti-phase flexor oscillations at low frequencies in symmetric conditions, which corresponds to a normal locomotor pattern. Therefore, our study provides additional support for the important role of V3 CINs and the existence of inhibitory commissural pathways from extensor half-centers to contralateral flexor half-centers, mediated by V3 and (presumably) V1 interneurons (10). Although this prediction still awaits experimental testing, crossed inhibition to flexors (by afferent stimulation) has been observed in anesthetized preparations (100, 101) and during locomotion in intact cats (76).

In summary, our analysis of the model allowed us to evaluate the specific roles of the two types of inhibitory commissural interactions (called here *flexor-flexor* and *extensor-flexor* inhibition) in left-right coordination. The flexor-flexor inhibition, presumably mediated by V0

CINs (12, 92), supports left-right alternation and its weakening may stabilize left-right in-phase synchronization. The extensor-flexor inhibition, presumably mediated by V3 CINs and V1 interneurons (10), ensures that left and right activities alternate in a strict out-of-phase manner in symmetric conditions.

3.6.3 Insights from symmetric locomotion

It is well known that during normal locomotion in cats and humans, an increase of speed is accompanied by a significant reduction of stance phase duration with or without a minor reduction of swing phase duration (4, 69, 70, 93, 94, 102) see also Fig. 3.3. This observation seems to support the flexor-driven concept of locomotor rhythm generation. However, in intact and spinal cats, increasing locomotor speed produces a more balanced pattern, with stance duration approaching and even becoming shorter than swing duration. This is clearly observed during overground locomotion in intact cats (Fig. 3.3A). We suggest that when approaching the point of equality between phases, rhythmogenesis shifts towards the classical half-center mechanism. There are two observations that indirectly support this view. First, we can see that after the point of equality, the oscillation period (and hence the frequency) saturates and does not change much, which is a typical feature of classical half-center dynamics (67, 96). Second, the fact that the extension/stance duration becomes shorter than flexion/swing duration (i.e. the flexor burst becomes shorter than the interburst intervals) contradicts existing models of flexor-driven locomotor activity (1).

3.6.4 Insights from asymmetric split-belt treadmill locomotion

Previous experimental studies in cats using split-belt treadmill locomotion demonstrated that the mammalian spinal cord has a remarkable adaptive capacity for left–right coordination, from simple to extreme conditions (4, 5, 9, 69, 93). In *simple* conditions, with slow/fast speed ratios of up to 1:2.5 (0.4:1.0 m/s), animals maintain the period of oscillations (and frequency) almost unchanged and compensate for the reduction of stance phase duration on the fast belt by a corresponding increase of the duration of the swing phase (4, 5); see Fig. 3.6. Our model was able to reproduce this feature specifically due to the implementation of our suggestion, that increased activation of the flexor half-center in each RG is accompanied by a reduction in the activity of the corresponding extensor half-center. This implementation leads to a switch in the rhythmogenic mechanism of the fast RG from flexor-driven oscillations to the classical half-center mechanism (Fig. 3.8A, B). Removing this feature from the model leads to constant swing duration accompanied by a noticeable increase of oscillation frequency in both limbs (RGs) with increasing drive to the flexor half-centers (Fig. 3.8C, D), contradicting the experimental results, shown in Fig. 3.6.

Experimental studies of cat locomotion on split-belt treadmills in *extreme conditions*, with slow/fast speed ratios of 1:3 and more (4, 68) showed that cats use a specific strategy to stabilize locomotion by taking multiple steps on the fast side per step on the slow side. Moreover, although there was some variability between animals, both intact (68) and spinal (4) cats exhibit 1:2, 1:3 or 1:4 coordination patterns corresponding to 2, 3 or 4 steps on the fast side per step on the slow side, respectively. To simulate these behaviors, we applied different drives to the left and right RGs in the model, assuming that these conditions are qualitatively similar to the extreme case of split-belt locomotion. Under these conditions, the model predicts that the number of different coordination

patterns depends on the value of the drive to the slow RG (Fig. 3.7). For relatively high drives to the slow RG (>0.45), only a 1:1 coordination pattern is possible, which corresponds to simple conditions in split-belt locomotion (see above). However, if the drive to the slow RG is smaller, 1:2+ coordination patterns become possible. For example, for a slow RG drive value of 0.4, as the drive to the fast RG increases, there is a transition from 1:1 to 1:2 coordination pattern, but no 1:3 regime exists, while for a slow RG drive value of 0.25, as the fast RG drive progressively increases, the system undergoes 1:1, 1:2, 1:3 and 1:4 regimes. Qualitatively similar behavior is observed in extreme split-belt locomotion where in order to achieve higher order coordination patterns, one has to set lower speeds of the slow belt.

3.6.5 Limitations, functional considerations, and future directions

In this study we show that a relatively simple functional connectome between populations of interneurons providing output to flexor and extensor motoneurons that control a pair of limbs can explain a variety of coordination patterns emerging in split-belt experiments. The mathematical model we developed allowed us to formulate a novel hypothesis about general mechanisms of locomotor phase duration control suggesting that variation of the excitatory drive to the flexor half-centers is accompanied by an opposite change in the drive to the extensor half-centers. However, our model does not provide any specifics on neuronal pathways mediating these interactions.

What would be the benefit of switching from a flexor-driven RG operation to a classic half-center mode with increasing speed? Although we can only speculate, the goal of the spinal locomotor network might be to optimize efficiency or balance (avoid falling). At slow to moderate speeds, the stance duration is long and inputs from group I/II extensor muscle afferents and paw

pad cutaneous afferents have a relatively long time to regulate stance duration and adjust/correct for destabilizing perturbations. Thus, at slow to moderate speeds, a flexor-driven RG mode is less costly and more efficient. However, as speed increases, stance duration also decreases and afferent inputs do not have as much time to adjust or correct for postural perturbations. As such, at high speeds, a classic half-center mode, whereby both stance and swing phase durations are balanced, becomes more efficient to avoid falling, as each phase can be more flexibly controlled.

Considering that similar coordination patterns are observed in split-belt experiments in both intact and spinal cats (4, 5), it is reasonable to assume that drives controlling left and right rhythm generators depend on sensory feedback rather than on supraspinal inputs. One obvious source of sensory feedback is muscle afferent inputs that are known to affect the dynamics of the spinal locomotor CPG (see (103) for review). Our model does not explicitly account for this type of feedback. Therefore, the functional interactions and intrinsic flexor and extensor half-centers' oscillatory properties can be defined in part by inputs from somatosensory afferents. Another type of sensory feedback known to influence locomotion is from the skin (76). Cutaneous feedback modulation by paw anesthesia alters margins of stability during split-belt cat locomotion (3). It was recently suggested that this alteration occurs due to misrepresentation of the center of mass in the cat's balance control system after disrupting cutaneous feedback from the paws (refer to the second chapter of this dissertation). Altogether, the balance control system and locomotor pattern generation may interact at the spinal level, which opens new ways to mathematically model these interactions and thus generate new hypotheses about neuronal pathways mapping somatosensory afferents to the spinal locomotor circuits. Decomposing the functional interactions between left and right RGs into components mediated by local commissural interneurons and spinal reflexes can be a major future research direction where mathematical modeling proves instrumental.

4 GENERAL DISCUSSION

Locomotion is an evolutionary adaptation that allows animals to move in 3-D space. Various types of locomotion exist, including swimming in aquatic animals, flying in aerial animals, and gaiting in terrestrial animals. We are interested in quadrupedal and bipedal locomotion of terrestrial mammals. Quadrupedal locomotion is the most common form of terrestrial locomotion in mammals and is used by cats, dogs, and human infants. Human adults move by bipedal locomotion.

The quadrupedal walking gait in human infants closely resembles the quadrupedal gait of mammals, such as cats, suggesting that the physiological architecture that produces these gaits in mammals is conserved in humans (104, 105). The results described in this dissertation are suggested to be extendable to the understanding of human locomotion although both are cat locomotion studies. The second chapter of this dissertation is about balance control, which is important for medical applications in humans, such as in spinal cord injury and in Parkinson's disease. The third chapter of this dissertation is about defining the connectivity of the nervous system network that controls locomotion. Understanding the connectivity of the network increases potential for rehabilitation from spinal cord injury.

4.1 The Power of Modeling

The locomotor CPG of invertebrates, such as the leech and the crayfish have been identified using biomolecular and electrophysiology techniques (106, 107). The mammalian locomotor CPG is difficult to study due to the limited knowledge of genetic markers for

locomotor CPG cells. Additionally, the spinal cord does not exhibit clear spatial organization of the CPG (52) with distribution of cells along different spinal segments. Optogenetic stimulation of interneurons of a specific type shows the necessity of these interneurons for specific gaits (1, 10, 61). In these studies, NMDA and 5-HT stimulate fictive locomotion and recordings of flexor and extensor activity are made during modulation of the activity of a particular interneuron. Because identification of all interneurons in the locomotor CPG is incomplete, additional tools are needed to outline the connectivity of the CPG network. We can confirm or eliminate a possible CPG connectivity by modeling the network and validating the behavior of the network against biological behavior. This method of validation has provided much knowledge about locomotor CPG interneurons to the scientific community (1, 10, 65, 67).

4.2 Our Conclusions and Future Directions

4.2.1 Conclusions and future directions from the second chapter, "Frontal Plane Dynamics of the Center of Mass During Quadrupedal Locomotion on a Split-Belt Treadmill"

In the second chapter of this dissertations, we model the center of oscillations of cats pacing on split-belt treadmills with an inverted pendulum model. We model the center of mass oscillations of pacing cats to study the balance control system.

During locomotion, the center of mass must stay within the edges of support, or limb positions in order to maintain balance. In pacing cats, ipsilateral limbs are lifted in unison and the

center of mass falls towards the lifted limbs. At some point in the lateral trajectory of the center of mass, the lifted limbs are placed on the ground and the opposing limbs are lifted to maintain balance. We find the threshold center of mass position at the moment of hind-limb lift (lateral stability thresholds) on each side of the body with an inverted pendulum model.

Our previous study of cat locomotion demonstrated that lateral displacements of center of mass were strikingly similar to those of human walking and resembled behavior of an inverted pendulum (3). We chose an inverted pendulum model because it allowed us to solve exactly for the amplitude, period, and average center of mass position. These parameters were fit to experimental data of cats walking on split-belt treadmills in different conditions in order to determine laterality threshold positions at each condition (3). In the experiments, the left and right belts of a split-belt treadmill are varied individually. Conditions included the progressive increase of the right belt speed while the left belt was held at a constant speed and a reverse condition in which the left belt speed was increased with respect to the right belt. With the speed perturbation, the center of mass shifts towards the slower belt. We find that the laterality threshold on the fast side shifts to a greater extent than on the slow side, which corresponds to earlier lift of the slow side limbs At each speed, cutaneous feedback was disrupted with anesthesia application to right paws and was compared to control. The center of mass shifts towards the anesthetized side with cutaneous feedback disruption. We find that laterality thresholds shift uniformly with anesthesia perturbation.

We believe that the center of mass shifts towards the anesthetized side because cutaneous feedback is necessary for determining the center of mass position. The difference in threshold shift on the left and right sides with unilateral anesthesia suggests that the central nervous system is involved in determining center of mass position.

The effect of anesthesia was found to depend on speed, with increasing effect on center of mass position with increasing speed. We believe this result reflects the use of multiple modalities to determine center of mass position. We suggest, that at high speeds the joint angle changes quickly and the signal from the joint becomes less reliable. Feedback from joints relies on incoming signals below the joint, while cutaneous feedback relies only on the pressure on the cutaneous sensors due to the weight of the body from gravity. Thus, at higher speeds, the cutaneous feedback from the bottoms of the paws may be more stable than feedback from joints. The nervous system may rely on cutaneous feedback to a greater extent at higher speeds, resulting in a greater error in center of mass position estimation and thus a greater shift in the center of mass as seen in experiment.

If joint input aids in determining center of mass position, then the center of mass will shift to a greater extent with joint feedback disruption. To this hypothesis, the series of experiments could be performed with joint vibration. An external vibrator may be attached to the joints and the experiments could be repeated for comparison. Vibration has been shown to disrupt signals from joints. If joint signals are disrupted with vibration and if the central nervous system relies on signals from the joints to determine center of mass position, then application of vibration to the joints will shift the center of mass.

It would also be interesting to repeat the series of experiments in this work, but with a decrease in speed of the right belt, instead of an increase in right belt speed. If joint receptors provide information about the center of mass that is distorted and unreliable at high speeds, then joint receptors should provide reliable feedback at slower speeds. This experiment also deciphers whether the effect of anesthesia is due to increase in speed or speed difference.

It is also possible that visual cues aid in determining center of mass position and that visual feedback becomes unreliable at high speeds. This hypothesis seems less reasonable because visual cues are constantly changing, independently of body position and thus determination of center of mass position should not rely on head position. In the future, it would be possible to test the hypothesis, that visual cues aid in determining center of mass position by repeating the aforementioned experiment and comparing results in light and dark conditions.

4.2.2 Conclusions and future directions from the third chapter, "On the organization of the locomotor CPG: insights from split-belt locomotion and mathematical modeling"

In the third chapter of this dissertation, we match the phases of flexion and extension in a locomotor CPG model to those of cats walking on split-belt treadmills. We model the CPG network to test the biological plausibility of a particular CPG network connectivity.

In the experiments by Frigon *et al.* 2017 (4), spinalized cats walked in tied-belt and in split-belt conditions. In tied-belt conditions, the speed of both left and right belts was increased in unison. In split-belt conditions, the speed of the right belt was increased individually and the left belt was held and a constant speed. Recordings from muscles that correspond to flexion and extension of each limb were made. The duration of flexion and extension was determined for each experimental condition by muscle recording and by video recording. In the tied-belt conditions, the duration of stance decreased, while the duration of swing stayed constant. In the split-belt conditions, the duration of stance decreased while the duration of swing increased in the right paw as right belt speed increased. The duration of stance and swing remained

approximately constant on the left side as it was kept at a constant speed. When the speed of the right belt was much higher than the left belt the right paws took multiple steps for each step on the left side.

A CPG network was formulated on the basis of a previously proposed network by Danner *et al.* 2019 (10). This network was simplified by combining excitatory and inhibitory connections, resulting in net inhibition in the reduced model. The model network consisted of one flexor half-center and one extensor half-center, that correspond to the neuronal populations that controls flexion and extension of two hind limbs. Half-centers consist of two neurons with mutual inhibition, such that only one half-center is active at a time (52). In our model, one of the half-centers corresponds to flexion of a hindlimb, while the other corresponds to extension the hindlimb, by projecting to corresponding flexion and extension motoneurons. The model also includes mutual inhibition between ipsilateral flexors and extensors and each extensor inhibits the contralateral flexor. We validated our proposed network connectivity by matching the duration of flexion and extension and the phase to the durations and phases seen in experiment. Our network produced multiple bursts on one side that correspond to multiple steps on one side of the split-belt treadmill in the experiments.

A burst (train of action potentials) of a flexor neuron corresponds to a single flexion of a limb, while a burst of an extensor neuron corresponds to extension of the limb. An external excitatory drive to each flexor increases the rate of bursting and simulated increased speed of walking. We find that the proposed network only reproduces the phases of flexion and extension seen in cats when increasing drive to flexor neurons is matched by decreasing drive to ipsilateral extensor neurons. This finding suggests the presence of an inhibitory interneuron that extends from external excitation to flexor neurons and inhibits extensor neurons.

It is unclear how the rhythm of switching between flexion and extension is generated. An important consideration to the generation of this rhythm is whether flexors and extensors burst intrinsically. An intrinsically busting cell generates bursts due to its intrinsic dynamics. It can be said that an intrinsically bursting cell sets a rhythm, or is a pacemaker. Some cells do not burst intrinsically, but do burst when they are coupled to other intrinsic bursters. Under the flexor-driven hypothesis, flexors burst intrinsically, while extensors do not burst intrinsically. In the quasisymmetric hypothesis, the rhythm is generated by mutual inhibition between flexors and extensors and neither flexors nor extensors set the pace. Alternatively, mutual inhibition may play a role in alternation between flexion and extension, but the rhythm could be set by intrinsic bursting of each flexors and extensors.

It is generally accepted that the CPG consists of two mutually-inhibiting half-center oscillators (54). In the classical half-center concept, each element of the half-center does not need to burst intrinsically because bursting occurs by adaptation that results in release from mutual inhibition (54, 57). Optogenetic studies have shown that rhythmic activity can be evoked in each flexors and extensors independently in certain conditions (61), suggesting that mutual inhibition need not be necessary for bursting activity. We suggest that both half-centers are conditional oscillators, which can burst intrinsically with the right amount of external excitation (12, 53, 66).

In our model the CPG can operate as a classical half-center, or be flexor-driven, depending on the level of external drive. According to the intrinsic dynamics of the cells in our model, cells are intrinsically bursting given a low external drive and spike tonically with a high external drive. Increase in drive to flexors is coupled by decrease in drive to extensors. When external drive to flexors is low they are intrinsically bursting, while drive to extensors is high and

they are tonically active. In this case, the system is flexor-driven. Increased speed of walking is simulated by an increase in drive to flexors and a corresponding decrease in drive to extensors. Increasing drive to flexors progressively increases frequency of flexor bursts and eventually resulting in a switch of states, where flexors enter a tonic mode. Higher drive to flexors is matched by a decrease in drive to extensors. With both flexors and extensors in tonic mode, the system behaves as a half-center oscillator. Thus, the connectivity of the CPG and the intrinsic dynamics of our cells are such that the system can switch from being flexor-driven to a classical half-center by an increase in external drive.

Frigon *et al.* found that the duration of stance phase decreases and swing phase increases when the speed of the right belt increases in spinalized cats walking on a split-belt treadmill (4). We find that our model can only reproduce a corresponding decrease in the duration of the extension phase and an increase in the duration of flexion if an increasing excitatory drive to flexors is accompanied by a decreasing drive to extensors. Our findings support the ability of the locomotor CPG to behave under the classical half-center concept, or be flexor-driven. We suggest that the neurons that control flexion and extension have intrinsic dynamics that make them conditional oscillators.

In our model, the decrease in drive to extensors that accompanies an increasing drive to flexors is implemented as a constant sum between the two drives. In the future, it would be interesting to explore our system with dynamic drives. We suggest the addition of an inhibitory interneuron between excitatory input to flexors and excitatory input to extensors. The exploration of the level of drive necessary to reproduce the results of Frigon *et al* 2017 with a dynamic drive would allow us to predict the relative level of drive native to the locomotor CPG.

The nature of the external excitatory drive in our model is not specified. Biologically, the external drive in our model can be considered as a descending command from the central nervous system, or as feedback from the periphery, such as cutaneous receptors, muscles, and joints. Spinalized cats do not receive descending commands from the central nervous system, but do receive feedback from the periphery, while intact cats receive descending commands from the central nervous system and feedback from the periphery. In both spinalized and intact cats, stance duration decreases and swing duration remains constant during tied-belt locomotion, but the change in stance duration with speed is greater in spinalized cats than in intact cats (4, 5). Similarly, stance duration decreases and swing duration increases during split-belt locomotion in both spinalized and intact cats, but the changes are greater in spinalized than in intact cats (4, 5). These results are shown in Fig. 3.3 and Fig. 3.6 in the third chapter of this dissertation. Our model reproduces these trends in swing and stance duration in tied-belt and in split-belt locomotion. In the future, we would like to explore the relative contribution of the central nervous system and feedback from the periphery to the increase in drive to the locomotor CPG by tuning our model to the precise change in swing and stance duration found in intact and in spinal cats. Specifically, the amount of external drive necessary to reproduce the changes in swing and stance duration for a given speed in spinalized cats is suggested to represent the external drive from the periphery. The amount of external drive necessary to reproduce the changes in swing and stance duration for a given speed in intact cats is suggested to represent the external drive that a combination of feedback from the periphery and the central nervous system.

REFERENCES

1. Molkov YI, Bacak BJ, Talpalar AE, Rybak IA. Mechanisms of left-right coordination in mammalian locomotor pattern generation circuits: a mathematical modeling view. PLoS Comput Biol. 2015;11(5):e1004270.

2. Kiehn O. Decoding the organization of spinal circuits that control locomotion. Nature Reviews Neuroscience. 2016;17(4):224.

3. Park H, Latash EM, Molkov YI, Klishko AN, Frigon A, DeWeerth SP, et al. Cutaneous sensory feedback from paw pads affects lateral balance control during split-belt locomotion in the cat. J Exp Biol. 2019;222(Pt 14).

4. Frigon A, Desrochers E, Thibaudier Y, Hurteau MF, Dambreville C. Left-right coordination from simple to extreme conditions during split-belt locomotion in the chronic spinal adult cat. The Journal of physiology. 2017;595(1):341-61.

5. Frigon A, Thibaudier Y, Hurteau M-F. Modulation of forelimb and hindlimb muscle activity during quadrupedal tied-belt and split-belt locomotion in intact cats. Neuroscience. 2015;290:266-78.

6. Wetzel MC, Atwater AE, Wait JV, Stuart DC. Neural implications of different profiles between treadmill and overground locomotion timings in cats. J Neurophysiol. 1975;38(3):492-501.

7. Farrell BJ, Bulgakova MA, Beloozerova IN, Sirota MG, Prilutsky BI. Body stability and muscle and motor cortex activity during walking with wide stance. Journal of neurophysiology. 2014;112(3):504-24.

8. Blaszczyk J, Loeb GE. Why cats pace on the treadmill. Physiol Behav. 1993;53(3):501-7.

9. Forssberg H, Grillner S, Halbertsma J, Rossignol S. The locomotion of the low spinal cat. II. Interlimb coordination. Acta Physiol Scand. 1980;108(3):283-95.

10. Danner SM, Zhang H, Shevtsova NA, Borowska-Fielding J, Deska-Gauthier D, Rybak IA, et al. Spinal V3 Interneurons and Left-Right Coordination in Mammalian Locomotion. Front Cell Neurosci. 2019;13:516.

11. Hof AL, Gazendam MG, Sinke WE. The condition for dynamic stability. J Biomech. 2005;38(1):1-8.

12. Shevtsova NA, Talpalar AE, Markin SN, Harris-Warrick RM, Kiehn O, Rybak IA. Organization of left–right coordination of neuronal activity in the mammalian spinal cord: Insights from computational modelling. The Journal of Physiology. 2015;593(11):2403-26.

13. Gray J. Studies in the Mechanics of the Tetrapod Skeleton. Journal of Experimental Biology. 1944;20(2):88-116.

14. Fung J, Macpherson JM. Determinants of postural orientation in quadrupedal stance. The Journal of neuroscience : the official journal of the Society for Neuroscience. 1995;15(2):1121-31.

15. Farrell BJ, Bulgakova MA, Sirota MG, Prilutsky BI, Beloozerova IN. Accurate stepping on a narrow path: mechanics, EMG, and motor cortex activity in the cat. Journal of neurophysiology. 2015;114(5):2682-702.

16. Usherwood JR, Szymanek KL, Daley MA. Compass gait mechanics account for top walking speeds in ducks and humans. J Exp Biol. 2008;211(Pt 23):3744-9.

17. Willener AS, Handrich Y, Halsey LG, Strike S. Fat King Penguins Are Less Steady on Their Feet. PloS one. 2016;11(2):e0147784.

18. Thompson NE, O'Neill MC, Holowka NB, Demes B. Step width and frontal plane trunk motion in bipedal chimpanzee and human walking. J Hum Evol. 2018;125:27-37.

19. MacKinnon CD, Winter DA. Control of whole body balance in the frontal plane during human walking. J Biomech. 1993;26(6):633-44.

20. O'Connor SM, Kuo AD. Direction-dependent control of balance during walking and standing. J Neurophysiol. 2009;102(3):1411-9.

21. Townsend MA. Biped gait stabilization via foot placement. J Biomech. 1985;18(1):21-38.

22. Hof AL, van Bockel RM, Schoppen T, Postema K. Control of lateral balance in walking. Experimental findings in normal subjects and above-knee amputees. Gait Posture. 2007;25(2):250-8.

23. Pai YC, Patton J. Center of mass velocity-position predictions for balance control. J Biomech. 1997;30(4):347-54.

24. Horak F, Macpherson J. Postural orientation and equilibrium. New York. Oxford; 1996.

25. Cavagna GA, Heglund NC, Taylor CR. Mechanical work in terrestrial locomotion: two basic mechanisms for minimizing energy expenditure. Am J Physiol. 1977;233(5):R243-61.

26. Griffin TM, Main RP, Farley CT. Biomechanics of quadrupedal walking: how do four-legged animals achieve inverted pendulum-like movements? J Exp Biol. 2004;207(Pt 20):3545-58.

27. Hildebrand M. Symmetrical gaits of dogs in relation to body build. J Morphol. 1968;124(3):353-60.

28. Dagg AI. The locomotion of the camel (Camelus dromedarius). Journal of Zoology. 1974;174(1):67-78.

29. Basu C, Wilson AM, Hutchinson JR. The locomotor kinematics and ground reaction forces of walking giraffes. J Exp Biol. 2019;222(Pt 2).

30. Pfau T, Hinton E, Whitehead C, Wiktorowicz-Conroy A, R. HJ. Temporal gait parameters in the alpaca and the evolution of pacing and trotting locomotion in the *Camelidae*. Journal of Zoology. 2011;283(3):193-202.

31. Hildebrand M. The Adaptive Significance of Tetrapod Gait Selection. American Zoologist. 1980;20(1):255-67.

32. Roden-Reynolds DC, Walker MH, Wasserman CR, Dean JC. Hip proprioceptive feedback influences the control of mediolateral stability during human walking. J Neurophysiol. 2015;114(4):2220-9.

33. Buurke TJW, Lamoth CJC, van der Woude LHV, Hof AL, den Otter R. Bilateral temporal control determines mediolateral margins of stability in symmetric and asymmetric human walking. Sci Rep. 2019;9(1):12494.

34. Buurke TJW, Lamoth CJC, Vervoort D, van der Woude LHV, den Otter R. Adaptive control of dynamic balance in human gait on a split-belt treadmill. J Exp Biol. 2018;221(Pt 13).

35. Ting LH, Macpherson JM. Ratio of shear to load ground-reaction force may underlie the directional tuning of the automatic postural response to rotation and translation. J Neurophysiol. 2004;92(2):808-23.

36. Bolton DA, Misiaszek JE. Contribution of hindpaw cutaneous inputs to the control of lateral stability during walking in the cat. J Neurophysiol. 2009;102(3):1711-24.

37. Perry SD, McIlroy WE, Maki BE. The role of plantar cutaneous mechanoreceptors in the control of compensatory stepping reactions evoked by unpredictable, multi-directional perturbation. Brain Res. 2000;877(2):401-6.

38. Meyer PF, Oddsson LI, De Luca CJ. Reduced plantar sensitivity alters postural responses to lateral perturbations of balance. Exp Brain Res. 2004;157(4):526-36.

39. Prilutsky BI, Sirota MG, Gregor RJ, Beloozerova IN. Quantification of motor cortex activity and full-body biomechanics during unconstrained locomotion. J Neurophysiol. 2005;94(4):2959-69.

40. Kuczynski V, Telonio A, Thibaudier Y, Hurteau MF, Dambreville C, Desrochers E, et al. Lack of adaptation during prolonged split-belt locomotion in the intact and spinal cat. J Physiol. 2017;595(17):5987-6006.

41. Finley JM, Bastian AJ, Gottschall JS. Learning to be economical: the energy cost of walking tracks motor adaptation. J Physiol. 2013;591(4):1081-95.

42. Torres-Oviedo G, Vasudevan E, Malone L, Bastian AJ. Locomotor adaptation. Prog Brain Res. 2011;191:65-74.

43. Mackenzie RA, Burke D, Skuse NF, Lethlean AK. Fibre function and perception during cutaneous nerve block. Journal of neurology, neurosurgery, and psychiatry. 1975;38(9):865-73.

44. Hogan QH, Abram SE. Neural blockade for diagnosis and prognosis. A review. Anesthesiology. 1997;86(1):216-41.

45. Manter JT. The dynamics of quadrupedal walking. Journal of Experimental Biology. 1938;15(4):522-40.

46. Macefield VG. Physiological characteristics of low-threshold mechanoreceptors in joints, muscle and skin in human subjects. Clin Exp Pharmacol Physiol. 2005;32(1-2):135-44.

47. Bouyer LJ, Rossignol S. Contribution of cutaneous inputs from the hindpaw to the control of locomotion. I. Intact cats. J Neurophysiol. 2003;90(6):3625-39.

48. Abraira VE, Ginty DD. The sensory neurons of touch. Neuron. 2013;79(4):618-39.

49. Strzalkowski NDJ, Peters RM, Inglis JT, Bent LR. Cutaneous afferent innervation of the human foot sole: what can we learn from single-unit recordings? J Neurophysiol. 2018;120(3):1233-46.

50. Musienko PE, Zelenin PV, Lyalka VF, Orlovsky GN, Deliagina TG. Postural performance in decerebrated rabbit. Behavioural brain research. 2008;190(1):124-34.

51. Musienko P, Courtine G, Tibbs JE, Kilimnik V, Savochin A, Garfinkel A, et al. Somatosensory control of balance during locomotion in decerebrated cat. J Neurophysiol. 2012;107(8):2072-82.

52. Rybak IA, Dougherty KJ, Shevtsova NA. Organization of the Mammalian Locomotor CPG: Review of Computational Model and Circuit Architectures Based on Genetically Identified Spinal Interneurons. eNeuro. 2015;2(5):ENEURO.0069-15.2015.

53. Danner SM, Shevtsova NA, Frigon A, Rybak IA. Computational modeling of spinal circuits controlling limb coordination and gaits in quadrupeds. eLife. 2017;6:e31050.

54. Brown TG. On the nature of the fundamental activity of the nervous centres; together with an analysis of the conditioning of rhythmic activity in progression, and a theory of the evolution of function in the nervous system. The Journal of physiology. 1914;48(1):18.

55. McCrea DA, Rybak IA. Organization of mammalian locomotor rhythm and pattern generation. Brain Res Rev. 2008;57(1):134–46.

56. Stuart DG, Hultborn H. Thomas Graham Brown (1882–1965), Anders Lundberg (1920–), and the neural control of stepping. Brain research reviews. 2008;59(1):74-95.

57. Wang XJ, Rinzel J. Alternating and Synchronous Rhythms in Reciprocally Inhibitory Model Neurons. Neural Computation. 1992;4(1):84-97.

58. Skinner FK, Kopell N, Marder E. Mechanisms for oscillation and frequency control in reciprocally inhibitory model neural networks. J Comput Neurosci. 1994;1(1-2):69-87.

59. Marder E, Bucher D. Central pattern generators and the control of rhythmic movements. Curr Biol. 2001;11(23):R986-96.

60. Marder E, Calabrese RL. Principles of rhythmic motor pattern generation. Physiol Rev. 1996;76(3):687-717.

61. Hägglund M, Dougherty KJ, Borgius L, Itohara S, Iwasato T, Kiehn O. Optogenetic dissection reveals multiple rhythmogenic modules underlying locomotion. Proceedings of the National Academy of Sciences. 2013;110(28):11589-94.

62. Duysens J. How deletions in a model could help explain deletions in the laboratory. J Neurophysiol. 2006;95(1):562-3; author reply 3-5.

63. Pearson K, Duysens J. Function of segmental reflexes in the control of stepping in cockroaches and cats. Neural control of locomotion: Springer; 1976. p. 519-37.

64. Duysens J, De Groote F, Jonkers I. The flexion synergy, mother of all synergies and father of new models of gait. Front Comput Neurosci. 2013;7:14.

65. Danner SM, Wilshin SD, Shevtsova NA, Rybak IA. Central control of interlimb coordination and speed-dependent gait expression in quadrupeds. J Physiol. 2016;594(23):6947–67.

66. Shevtsova NA, Rybak IA. Organization of flexor–extensor interactions in the mammalian spinal cord: insights from computational modelling. The Journal of physiology. 2016;594(21):6117-31.

67. Ausborn J, Snyder AC, Shevtsova NA, Rybak IA, Rubin JE. State-dependent rhythmogenesis and frequency control in a half-center locomotor CPG. J Neurophysiol. 2018;119(1):96-117.

68. Kuczynski V, Telonio A, Thibaudier Y, Hurteau MF, Dambreville C, Desrochers E, et al. Lack of adaptation during prolonged split-belt locomotion in the intact and spinal cat. The Journal of physiology. 2017;595(17):5987-6006.

69. Frigon A, Hurteau M-F, Thibaudier Y, Leblond H, Telonio A, D'Angelo G. Split-belt walking alters the relationship between locomotor phases and cycle duration across speeds in intact and chronic spinalized adult cats. Journal of Neuroscience. 2013;33(19):8559-66.

70. Frigon A, D'Angelo G, Thibaudier Y, Hurteau MF, Telonio A, Kuczynski V, et al. Speed-dependent modulation of phase variations on a step-by-step basis and its impact on the consistency of interlimb coordination during quadrupedal locomotion in intact adult cats. J Neurophysiol. 2014;111(9):1885-902.

71. Hurteau MF, Thibaudier Y, Dambreville C, Desaulniers C, Frigon A. Effect of stimulating the lumbar skin caudal to a complete spinal cord injury on hindlimb locomotion. J Neurophysiol. 2015;113(2):669-76.

72. D'Angelo G, Thibaudier Y, Telonio A, Hurteau MF, Kuczynski V, Dambreville C, et al. Modulation of phase durations, phase variations, and temporal coordination of the four limbs during quadrupedal split-belt locomotion in intact adult cats. J Neurophysiol. 2014;112(8):1825-37.

73. Dambreville C, Labarre A, Thibaudier Y, Hurteau MF, Frigon A. The spinal control of locomotion and step-to-step variability in left-right symmetry from slow to moderate speeds. J Neurophysiol. 2015;114(2):1119-28.

74. Thibaudier Y, Frigon A. Spatiotemporal control of interlimb coordination during transverse split-belt locomotion with 1:1 or 2:1 coupling patterns in intact adult cats. J Neurophysiol. 2014;112(8):2006-18.

75. Thibaudier Y, Hurteau MF, Telonio A, Frigon A. Coordination between the fore- and hindlimbs is bidirectional, asymmetrically organized, and flexible during quadrupedal locomotion in the intact adult cat. Neuroscience. 2013;240:13-26.

76. Hurteau MF, Thibaudier Y, Dambreville C, Danner SM, Rybak IA, Frigon A. Intralimb and Interlimb Cutaneous Reflexes during Locomotion in the Intact Cat. J Neurosci. 2018;38(17):4104-22.

77. Hurteau MF, Frigon A. A Spinal Mechanism Related to Left-Right Symmetry Reduces Cutaneous Reflex Modulation Independently of Speed During Split-Belt Locomotion. J Neurosci. 2018;38(48):10314-28.

78. Harnie J, Cote-Sarrazin C, Hurteau MF, Desrochers E, Doelman A, Amhis N, et al. The modulation of locomotor speed is maintained following partial denervation of ankle extensors in spinal cats. J Neurophysiol. 2018;120(3):1274-85.

79. Hurteau MF, Thibaudier Y, Dambreville C, Chraibi A, Desrochers E, Telonio A, et al. Nonlinear Modulation of Cutaneous Reflexes with Increasing Speed of Locomotion in Spinal Cats. J Neurosci. 2017;37(14):3896-912.

80. Dambreville C, Charest J, Thibaudier Y, Hurteau MF, Kuczynski V, Grenier G, et al. Adaptive muscle plasticity of a remaining agonist following denervation of its close synergists in a model of complete spinal cord injury. J Neurophysiol. 2016;116(3):1366-74.

81. Thibaudier Y, Hurteau MF, Dambreville C, Chraibi A, Goetz L, Frigon A. Interlimb Coordination during Tied-Belt and Transverse Split-Belt Locomotion before and after an Incomplete Spinal Cord Injury. J Neurotrauma. 2017;34(9):1751-65.

82. Desrochers E, Harnie J, Doelman A, Hurteau MF, Frigon A. Spinal control of muscle synergies for adult mammalian locomotion. The Journal of physiology. 2019;597(1):333-50.

83. Kilkenny C, Browne WJ, Cuthill IC, Emerson M, Altman DG. Improving bioscience research reporting: the ARRIVE guidelines for reporting animal research. PLoS Biol. 2010;8(6):e1000412.

84. Grundy D. Principles and standards for reporting animal experiments in The Journal of Physiology and Experimental Physiology. The Journal of physiology. 2015;593(12):2547-9.

85. Ermentrout B. Reduction of Conductance-Based Models with Slow Synapses to Neural Nets. Neural Comput. 1994;6(4):679-95.

86. Rybak IA, Shevtsova NA, Kiehn O. Modelling genetic reorganization in the mouse spinal cord affecting left-right coordination during locomotion. The Journal of physiology. 2013;591(Pt 22):5491-508.

87. Ausborn J, Shevtsova NA, Caggiano V, Danner SM, Rybak IA. Computational modeling of brainstem circuits controlling locomotor frequency and gait. Elife. 2019;8.

88. Rubin JE, Shevtsova NA, Ermentrout GB, Smith JC, Rybak IA. Multiple Rhythmic States in a Model of the Respiratory Central Pattern Generator. Journal of Neurophysiology. 2009;101(4):2146-65.

89. Molkov YI, Shevtsova NA, Park C, Ben-Tal A, Smith JC, Rubin JE, et al. A closed-loop model of the respiratory system: focus on hypercapnia and active expiration. PLoS One. 2014;9(10):e109894.

90. Molkov YI, Rubin JE, Rybak IA, Smith JC. Computational models of the neural control of breathing. Wiley Interdiscip Rev Syst Biol Med. 2016.

91. Rubin JE, Bacak BJ, Molkov YI, Shevtsova NA, Smith JC, Rybak IA. Interacting oscillations in neural control of breathing: modeling and qualitative analysis. J Comput Neurosci. 2011;30(3):607-32.

92. Talpalar AE, Bouvier J, Borgius L, Fortin G, Pierani A, Kiehn O. Dual-mode operation of neuronal networks involved in left-right alternation. Nature. 2013;500(7460):85-8.

93. Halbertsma JM. The stride cycle of the cat: the modelling of locomotion by computerized analysis of automatic recordings. Acta physiologica Scandinavica Supplementum. 1983;521:1-75.

94. Frigon A, Gossard JP. Asymmetric control of cycle period by the spinal locomotor rhythm generator in the adult cat. The Journal of physiology. 2009;587(Pt 19):4617-28.

95. Kulagin A, Shik M. Interaction of symmetrical limbs during controlled locomotion. Biophysics. 1970.

96. Daun S, Rubin JE, Rybak IA. Control of oscillation periods and phase durations in half-center central pattern generators: a comparative mechanistic analysis. J Comput Neurosci. 2009;27(1):3-36.

97. Jasinski PE, Molkov YI, Shevtsova NA, Smith JC, Rybak IA. Sodium and calcium mechanisms of rhythmic bursting in excitatory neural networks of the pre-Botzinger complex: a computational modelling study. Eur J Neurosci. 2013;37(2):212-30.

98. Pearson KG. Proprioceptive regulation of locomotion. Curr Opin Neurobiol. 1995;5(6):786-91.

99. Dietz V, Duysens J. Significance of load receptor input during locomotion: a review. Gait & posture. 2000;11(2):102-10.

100. Jankowska E, Edgley SA. Functional subdivision of feline spinal interneurons in reflex pathways from group Ib and II muscle afferents; an update. Eur J Neurosci. 2010;32(6):881-93.

101. Jankowska E, Edgley SA, Krutki P, Hammar I. Functional differentiation and organization of feline midlumbar commissural interneurones. The Journal of physiology. 2005;565(Pt 2):645-58.

102. Grillner S, Brookhart M, Mountcastle V. Handbook of Physiology, section 1, The Nervous System, vol. II, Motor Control. American Physiological Society; 1981.

103. Markin SN, Klishko AN, Shevtsova NA, Lemay MA, Prilutsky BI, Rybak IA. Afferent control of locomotor CPG: insights from a simple neuromechanical model. Annals of the New York Academy of Sciences. 2010;1198:21-34.

104. Righetti L, Nylén A, Rosander K, Ijspeert AJ. Kinematic and gait similarities between crawling human infants and other quadruped mammals. Frontiers in neurology. 2015;6:17.

105. Thelen E, Ulrich BD, Niles D. Bilateral coordination in human infants: stepping on a split-belt treadmill. Journal of Experimental Psychology: Human Perception and Performance. 1987;13(3):405.

106. Cymbalyuk GS, Gaudry Q, Masino MA, Calabrese RL. Bursting in leech heart interneurons: cell-autonomous and network-based mechanisms. Journal of Neuroscience. 2002;22(24):10580-92.

107. Cattaert D, Le Ray D. Adaptive motor control in crayfish. Progress in neurobiology. 2001;63(2):199-240.